Wireless Passive Substrate-Integrated Waveguide (SIW) Resonator-Based E-Field Sensor and Its Application to Monitor High-Voltage Apparatus

by

Amirmasoud Amirkabiri

A Thesis submitted to the Faculty of Graduate Studies of
The University of Manitoba
in partial fulfilment of the requirements of the degree of

Master of Science

Department of Electrical and Computer Engineering
University of Manitoba
Winnipeg, Canada

Examining Committee

This thesis was examined and approved by the following examining committee on March 26, 2018:

- **Prof. B. Kordi** (advisor)

  Department of Electrical & Computer Engineering

  University of Manitoba

- **Prof. G. E. Bridges** (co-advisor)

  Department of Electrical & Computer Engineering

  University of Manitoba

- **Prof. D. Isleifson**

  Department of Electrical & Computer Engineering

  University of Manitoba

- **Prof. M. Khoshdarregi**

  Department of Mechanical Engineering

  University of Manitoba

Abstract

In this thesis, a passive electric field sensor based on a substrate-integrated waveguide (SIW) resonator is designed, fabricated, and evaluated in the measurement of electric field of high voltage produced by two parallel plates. The proposed sensor is potentially applicable to measure the electric field of the high voltage apparatus remotely. When exposed to an external electric field, the resonance frequency of the SIW resonator-based sensor changes due to the variation of the capacitance of diode varactors that are mounted on the sensor. The capacitance of the varactor diode is a function of the voltage induced in its terminals. The sensor is designed to work in the industrial, scientific and medical (ISM) radio frequency band and demonstrates a high loaded quality factor of more than 200. An interrogation system has been developed that is capable of measuring the time-varying resonance frequency of the proposed sensor and deriving the waveform of the external electric field. The interrogation system transmits pulses of radio frequency (RF) signals to the sensor and the sensor re-emits the decaying ring back signals. The recorded ring back signals are downconverted and analyzed to derive the resonance frequency of the sensor.

Acknowledgements

Firstly, I would like to express many thanks to my advisor Dr. Behzad Kordi for his guidance and patience through my M.Sc. His brilliant advice and support during my studies encourage me to keep going. I would also like to express my gratitude to my co-advisor, Dr. Gregory. E. Bridges for his exceptional suggestions and comments through my thesis. His passion toward his job is a wonderful encouragement for young engineers and scientists.

Many thanks to my thesis committee, Dr. Dustin Isleifson and Dr. Mohammad Khoshdarregi for their comments and suggestions to improve my thesis.

I am also grateful to Daryl Hamelin, Cory Smit, Zoran Trajkoski for their kind help and practical knowledge to solve the problems we faced during the thesis at the laboratory.

Financial support from faculty of graduate studies and Natural Sciences and Engineering Research Council of Canada (NSERC) is gratefully acknowledged.

Last but definitely not least, I would like to thank my family and friends. Many sincere thanks to my lovely parents, Akram Sabati Azari and Mansour Amirkabiri for their kindness and patience and their entire support while I was pursuing my studies away from them. Without my parents encouragement, I would have never been able to follow my dreams. Many thanks to my second family here in lovely Winnipeg, Hassan, Narges and their lovely daughter, Parmin. They welcomed me in my very first days here and support me to commence a life as a newcomer. I am also grateful to dear Sanaz and Ehsan for always being there to help me and their encouragement and advice while I was trying to write my thesis.

Dedication

To my lovely, supportive mother and father,

to whom who believes in justice and fights for a world with more justice,

to whom who dares to explore and goes beyond the limits.

Table of Contents

List of Figures

List of Tables

Chapter 1

Introduction

1.1 Background

The recent growing demand in electric power has arisen the necessity of high voltage apparatus with high quality. Consequently, to avoid any probable power instabilities, maintenance of the high voltage apparatus requiring monitoring conditions of devices and protection against any defects is vital.

Electric field assessment around the high voltage apparatus is a viable candidate for condition monitoring of power systems. The distribution of the electric field reveals probable defects that might have been created. The collected information can be used to enhance personnel safety and improve maintenance as well.

Due to safety issues, direct contact with high voltage equipment is a hazardous situation. Therefore, to avoid the unsafe conditions, contactless measurement using wireless sensors is desirable where there is no direct contact between the sensor and the high voltage apparatus.

Recent advances in the development of wireless passive resonator-based sensors have expanded their industrial applications [1–5]. Their benefit of being wireless is a key factor to employ them where human contact is not appropriate [6–8]. The sensor is passive which means it is not required to have batteries. Being wireless means the sensor is capable of being interrogated remotely without being close to the high voltage apparatus. The resonance frequency of such sensors varies when there is a change in the parameter to be measured.

1.2 Problem Definition and Conventional Solutions

Existing measurement techniques for high voltage devices are established based on voltage dividers and transformers. These techniques require direct contact to the high voltage apparatus and decrease the current or voltage of the high voltage measurand in order to be measured as low voltage measurand. Direct human contact while dealing with the high voltage apparatus for condition monitoring is not desired. The value of the induced electric field as a result of the significant voltage difference between the high/medium voltage equipment and the grounding, is high enough to be hazardous to humans .

These techniques disturb voltage (which is to be measured) and de-energization which is not preferable. In addition, the techniques mentioned above modify source loading and their power consumption is not negligible. Voltage dividers utilized in this application are composed of massive capacitors, resistors or inductors. Their configuration not only adds physical limitations, but also causes some performance limitations such as transformer saturation. Another major issue is related to the induction of ferro-resonance in power systems due to the need to employ transformers in high voltage measurements [9] [10].

In order to monitor the condition of a high voltage apparatus, sensors and probes are utilized for measuring the electric field surrounding high voltage apparatus. Many of the sensors and probes such as optical sensors, electrostatic probes, Micro-electro-mechanical-system sensors, capacitive or inductive coupled sensors are active and require batteries. Some of the reported sensors above require direct contact using wires and the others are capable of measuring remotely. For remote measurements, an interrogation system is required to derive the proxy to be measured in order to obtain the electric field. The interrogation system reported in [11] is based on sending a pulsed radio frequency (RF) signals and receives the re-emitted ring back signals of the resonator-based sensor. The received ring back signals are utilized to derive the resonance frequency of the sensor. Interrogation systems are employed that are based on either near-field coupling [5], [12] or radiative back scattering [13–15].

Most existing passive, wireless sensor systems are developed for the measurement of quasi-static measurands (e.g. humidity, pressure, temperature) and are not able to measure time-varying measurands. The proposed sensor and the the interrogation system is capable of measuring time-varying measurands with fast sampling rate. This will allow to monitor the electric field surrounding the high voltage apparatus.

1.3 Objective of the Thesis

The objective of this thesis project is to design and fabricate a resonator-based wireless passive sensor and the corresponding interrogation system. The application discussed in this study is to measure the AC electric field near high voltage apparatus using the proposed resonator-based sensor. Substrate-integrated waveguide (SIW) technology is employed to achieve a high quality factor sensor. The SIW offers the high quality factor advantage of the non-planar waveguides in compatibility with planar structures. Thus, printed circuit board (PCB) fabrication methods can be used to fabricate the SIW resonator-based sensor.

The sensor consists of an SIW resonator loaded with varactor diodes. The varactor diodes are lumped elements. The capacitance of the varactors is a function of the voltage applied to their terminals. An external electric field coupled to the sensor imposes induced voltage over the terminals and varies the capacitance resulting in a resonance frequency shift of the SIW sensor.

The proposed SIW sensor is light-weight and has small dimensions. It is also easy to fabricate which allows commercial mass-production.

A compatible interrogation system with the proposed sensor is implemented in this work. The interrogation system is capable of sensing time-variant signals. This offers monitoring the AC

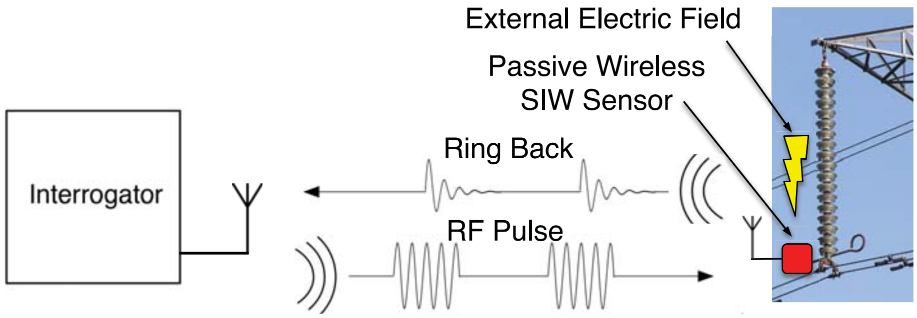

Fig. 1.1: Schematic of the operation fundamentals of the proposed wireless passive sensor.

electric field of the high voltage apparatus.

The sensor is passive which means there is no need for batteries. It is also wireless which allows remote interrogation wherever human contact is not desired.The SIW sensor does not need to be grounded and it can be located in close distance to the high voltage apparatus. Therefore, the proposed sensor is a viable candidate for condition monitoring of high voltage equipment such as live-maintenance of the high-voltage transmission lines, transformers and insulation deficiencies. Fig. 1.1 represents a schematic of the operation fundamentals of the passive, wireless sensor. The sensor is located in the vicinity of the high voltage apparatus to assess the electric field surrounding the high voltage apparatus. The interrogator system is sending pulses of radio frequency (RF) signals to the passive wireless electric field sensor. The passive wireless sensor is re-emitting pulses of the decaying sine wave (ring back signals) to the interrogation system. This mechanism provides the remote interrogation of the resonator-based sensor.

1.4 Research Contributions

The contributions of this thesis are as follows:

- Substrate-integrated waveguide (SIW) resonator is designed and simulated using the finite element method. The proposed design is examined precisely by simulation and the parameters such as the radius of the isolated region, the coupling distance, the insertion depth of the microstrip transmission line, *etc.* that affect the quality factor and energy coupling are optimized.

- An SIW resonator, with a coupling microstrip transmission line to energize the resonator, is used to fabricate a novel resonator-based sensor to monitor a high voltage apparatus condition remotely.
- Substrate-integrated waveguide technology has the advantages of both non-planar classic rectangular waveguide and planar structure on one platform simultaneously. This allows to achieve high quality factor on planar structures such as microstrip transmission lines. Thus, it is easy-to-fabricate and inexpensive resulting in commercial mass-production.
- Unlike the conventional methods using bulky voltage dividers and transformers, the proposed sensor is light-weight and relatively small in size. Therefore, it offers portability and it can be easily used in arrays along the distributed high voltage apparatus.
- Most of the existing solutions for condition monitoring of high voltage apparatus are either based on energy harvesting from the high voltage apparatus or require direct contact in order to assess the voltage or current. In other words, source loading is a major issue of the conventional condition monitoring solutions. The proposed sensor is capable of being interrogated remotely without any disturbance of the high voltage or power dissipation.
- Recently, some sensors have been introduced to derive only the Root Mean Square (RMS) value of the measured voltage or current. The proposed sensor is capable of measuring time-varying AC electric fields.
- The proposed sensor is workable remotely. In order to monitor an AC electric field, an interrogation system capable of measuring time-variant measurands is required. The interrogation system introduced in [11] was utilized in this study. The interrogation system is made up

of radio frequency (RF) sources, switches, amplifiers, DC blocks, a mixer, a coupler and a low-pass filter. It is based on sending RF pulses to energize the sensor and receive the ring back signals re-emitted from the sensors.

- The proposed SIW resonator-based sensor offers a wider tunability for frequency shift in comparison to the existing resonator-based sensor such as the coaxial sensor in [11]. Therefore, it offers a higher sensitivity resulting in more accuracy in measurements. Moreover, the dimension of the proposed sensor is smaller as well.

1.4.1 Publications

The outcome of this study has been submitted as a conference paper to International Symposium on Electromagnetic Compatibility (EMC EUROPE 2018). The main focus of the paper is on the design, fabrication, and assessment of the SIW resonator-based sensor to monitor the AC electric field generated by two parallel plates.

1.5 Thesis Outline

This thesis is classified into 5 chapters as defined below:

Chapter 1: Introduction, background information, problem definition and existing solutions, objectives, and contributions.

Chapter 2: Literature review of this study completed on Substrate-Integrated Waveguide (SIW) structures and their tunability, existing sensor to monitor high voltage apparatus and measure electric field in the vicinity of the high voltage devices and specifically passive wireless sensors. This chapter also includes interrogation systems utilized to obtain the information provided by the sensors.

Chapter 3: Discussion on the design procedure and computer simulation technique applied to optimize the proposed SIW resonator-based sensor.

Chapter 4: Discussion on the fabrication of the different prototypes of SIW resonator- based sensor and S-parameter analysis of the prototypes using Vector Network Analyzer (VNA) to observe frequency shift caused by applying direct DC biasing reverse voltages on terminals of the varactor diode.

Chapter 5: Discussion on the methodology of interrogating the SIW sensor remotely. Experimental Results of the the resonance frequency determination and re-constructed signal waveforms are presented for different fabricated prototypes. The results of the re-constructed external electric field generated by two parallel plates are illustrated as well.

Chapter 6: Conclusion of this thesis project, with a discussion on future work.

Chapter 2

Literature Review

2.1 Substrate-Integrated Waveguide Technology

Substrate-integrated waveguide technology has been an emerging alternative for rectangular metallic waveguides since it was introduced in [16] and [17]. Novel applications of this technology in various industrial and medical areas, such as biomedical applications, radars and networks, resulted in low-cost production for commercial applications.

An emerging trend is to investigate a single platform upon which all components can be implemented. The proposed platform has to be cost-effective, easy-to-fabricate and consistent high performance. One of the promising solutions presented is the substrate-integrated waveguide (SIW) methodology.

Substrate-integrated waveguides consist of conducting cylinders or slots located through dielectric material which bond conducting slots substitute the metallic walls of non-planar regular metallic waveguides as shown in Fig. 2.1. Current planar fabrication methods, such as printed circuit board (PCB) or low-temperature co-fired ceramic (LTCC) technology, enable the fabrication of waveguide structures in a planar form that is compatible with non-planar structures. It is possible to make cavities out of the SIW by blocking two edges of the structure similar to the process for rectangular non-planar waveguides. It is worth mentioning that the characteristics of SIW technology is almost the same as that of the existing non-planar rectangular waveguide technology.

Consequently, some similar criteria (to be discussed later) can be satisfied and taken into account. For instance, the field pattern of electromagnetic waves propagating in an SIW, is identical to that of the rectangular waveguide. The high-quality factor, electrical isolation, high-power handling are features of both SIW structures and classic rectangular waveguides. The substrate-integrated waveguide method not only preserves the characteristics of rectangular waveguide but also provides the capability of integrating all passive and active components and antennas on the same substrate as the desired unique platform. This provides the ability to remove transient mediums between different fabrication techniques which cause unwanted parasitic effects and losses. The concept of System on Substrate (SoS) was therefore introduced as an alternative on System in Package (SiP) to fabricate microwave systems.

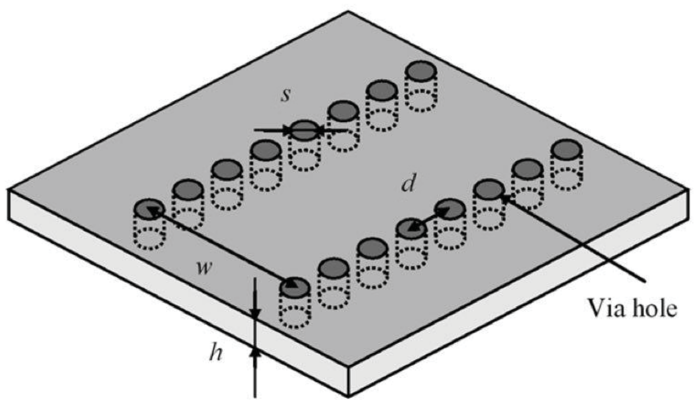

Fig. 2.1: Configuration of an SIW structure adopted from [19] ©2005 IEEE.

First, the concept of substrate-integrated waveguide was presented for post-wall waveguide [16] and laminated waveguide [17] . Later, the leakage behaviour of the method was discussed [19]. Deslandes et al developed a detailed modelling of substrate-integrated waveguide structure, including design considerations and criteria, and the mechanism of wave propagation that will be also discussed [20].

The application of the SIW method to fabricate microwave components has been reported in a number of studies including those that involve directional couplers, power amplifiers, voltage-controlled oscillators, cavity filters, slot-array, and other antennas and circulators. High quality resonators play a key role in fabricating many of the passive and active microwave and components. Therefore, by having a promising high-Q, SIW structures have the potential of being incorporated in such components. Most of the fabricated SIW structures work up to 30 GHz and a few of them have been reported to operate at higher frequencies [21]. Fabricating substrate-integrated waveguide components at higher frequencies is an issue, as it is challenging to find a practical substrate with reasonably low loss at higher frequencies to maintain the high quality factor.

Overall, SIW Structures have the advantages of both non-planar (three-dimensional) waveguides and planar waveguides simultaneously listed below:

1. High Quality factor in comparison to planar waveguides.
2. Capability of high-power performance.
3. Electrical isolation provided by conducting via posts (slots).
4. Compatible with the integration of passive and active components and antennas.

Due to the relative permittivity of the substrate utilized in the fabrication of the SIW, as well as its thickness, the high-power handling of the SIW structures is limited, but the production output is still able to perform in high-power situations. It is worth mentioning that the advantage No.4 is the main reason that the resonators are developed on PCB using the substrate-integrated waveguide technology.

2.1.1 Tunable SIW Structures

The high quality factor of SIW structures (higher than 200) results in a narrow bandwidth. In some applications, the narrow bandwidth and high selectivity is desired. However some applications are in need of wider coverage of frequency sweeping. In those cases tuning the SIW after its fabrication, even for devices with narrow bandwidth and high selectivity, may be required to achieve the aimed operating frequency. Additionally, multi-channel components operate in different frequency bands simultaneously. A drawback to using multi-channel components is the interference and cross-talk from other frequency channels. Tunable SIW Structures offer better isolation and can be a more suitable candidate for fabrication. When designing Tunable SIW Structures the tuning option should not decrease the selectivity and Q-factor of the SIW structure dramatically.

Listed below are several applications of tunable substrate-integrated waveguide structures that have been reported in previous studies: [18]:

1. Tunable Antennas [22–24]
2. Tunable resonator-based voltage-controlled oscillators(VCO) [25–28]
3. Tunable filters [29–33]
4. Phase shifters and isolators [34–40]

The components used in above applications are fabricated using substrate-integrated waveguide resonators that involves tuning methods of SIW resonators. The classic rectangular waveguide tuning is not applicable to SIW resonators. There have been several methods presented to tune an SIW resonator. Some of these methods are based on changing the electrical characteristics of the SIW resonator, while the others are based on changing mechanical or magnetic features [18].

To have frequency tuning, some methods (discussed later) use radio frequency microelectromechanical systems (RF-MEMS) switches, positive-intrinsic-negative (p-i-n) diodes, varactor diodes, and magnetic or mechanical switches [18]. One of the methods, introduced in [41], uses the varactor diode coupled with one of the walls of the SIW resonator. The walls are where the electric field is at minimum; therefore the effect of coupling will be minimum and the tuning range will be small as well. On the other hand, it will not disturb the high selectivity and quality factor of the proposed SIW bandpass filter [41].

The tuning method reported in [22] uses a metalized via post going through the substrate and connects to the top patch. The positive-intrinsic-negative (p-i-n) diodes and RF MEMS switches are both connected to the top plate. By connecting the metalized via post to the top plate (once the diode/switch is on) the metalized via post changes the electric field distribution which results

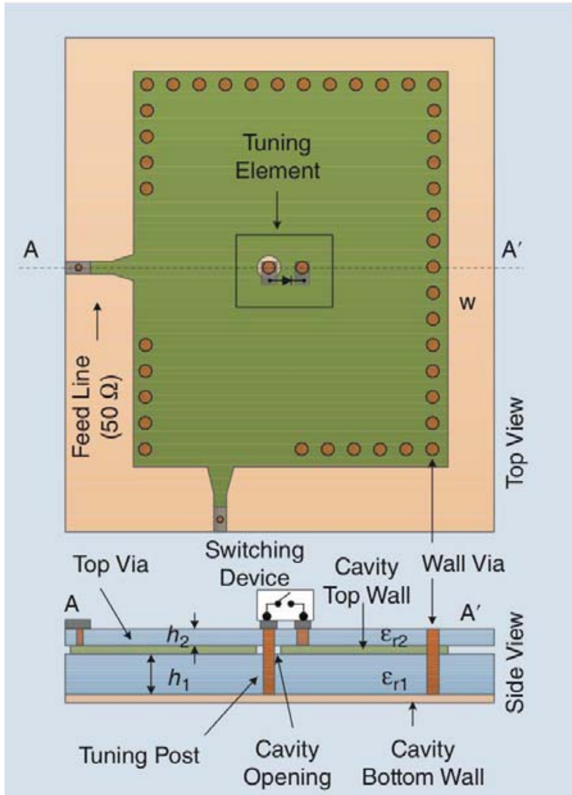

Fig. 2.2: Schematic of the tuning method of the via post-loaded SIW resonator adopted from [18] ©2015 IEEE.

in a frequency shift. The post is not connected to the top patch while it is off, resulting in a gap between them. This gap might effect the capacitance of the resonator but its effect is almost negligible. This structure is shown in Fig. 2.2 where the structure consists two layers of different substrates.

Sirci et al [42] presented a new method based on a floating area shown in Fig. 2.3 on the top patch which is connected by a metalized via post to the ground plate. A varactor diode is used to connect the floating area to the rest of the top patch. This method employs the variation of frequency by perturbating the electric field where it is close to its maximum magnitude. On the other hand, since the reverse bias voltage of the varactor diode can be varied, it allows the structure

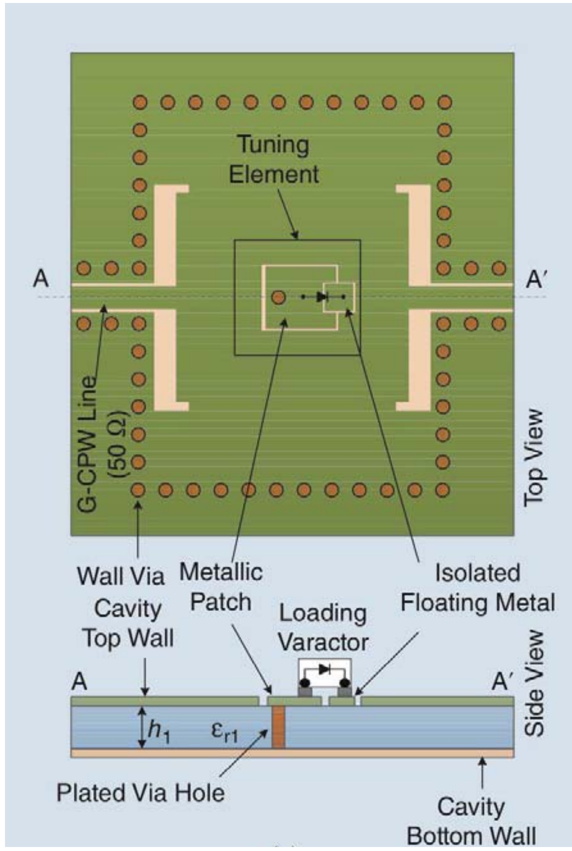

Fig. 2.3: Schematic of the tuning method of the SIW structure using the floating area loaded with a varactor diode adopted from [18] ©2015 IEEE.

to reactively change the operating frequency. Although the structure has one layer and it is easy to fabricate, the method illustrated in [42] can operate at frequencies from on 2.6 to 3.1 GHz and the quality factor reported is 40 to 160, which is not high enough for wireless interrogation and far-field measurements using antennas.

It is also possible to perform tuning by modifying the magnetic and electric field simultaneously. Inserting ferrite in the substrate, as shown in Fig. 2.4, is an option to achieve an optimization of loss tangent and quality factor of the structure as well. An external magnetic field can also cause a deviation of H-field distribution of the resonator which results in a frequency shift. Additionally, this

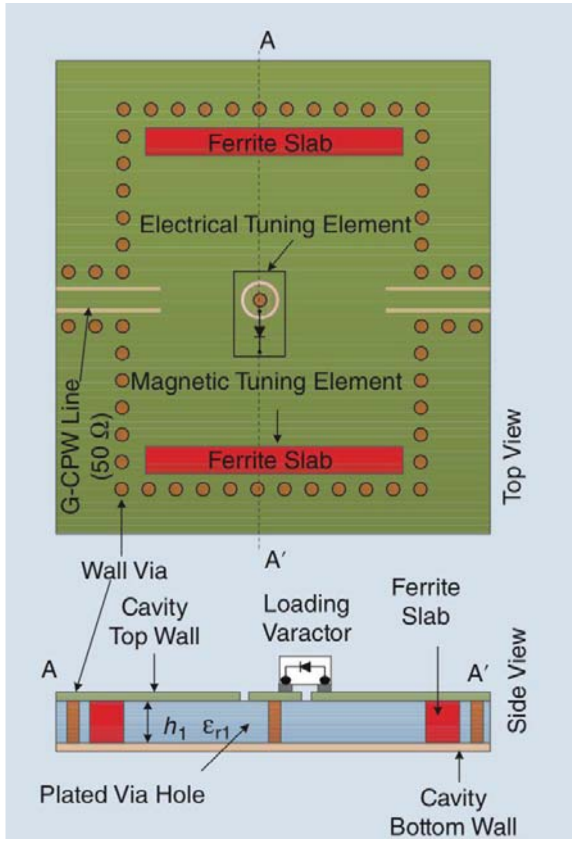

Fig. 2.4: Schematic of the tuning method of SIW structure using ferrite disks adopted from [18] ©2015 IEEE.

tuning method also offers an option to monitor magnetic field changes using a substrate-integrated waveguide structure. In comparison to the former methods, it is challenging to insert the ferrite units inside the substrate. By adding multiple magnetic material, units it becomes practical to improve the performance of magnetic field detection and to achieve a wide tuning range [34], [43].

An other approach is mechanical tuning via post structure using a screw. As shown in Fig. 2.5 the screw is connected to a flap. The screw is not connected directly to the top patch, but a ring is used to isolate the region between them. By turning the screw at different angles the resonance frequency varies due to a perturbed distribution of electric field [44].

The last method that is reported in [45] is based on isolated regions provided by ring gaps

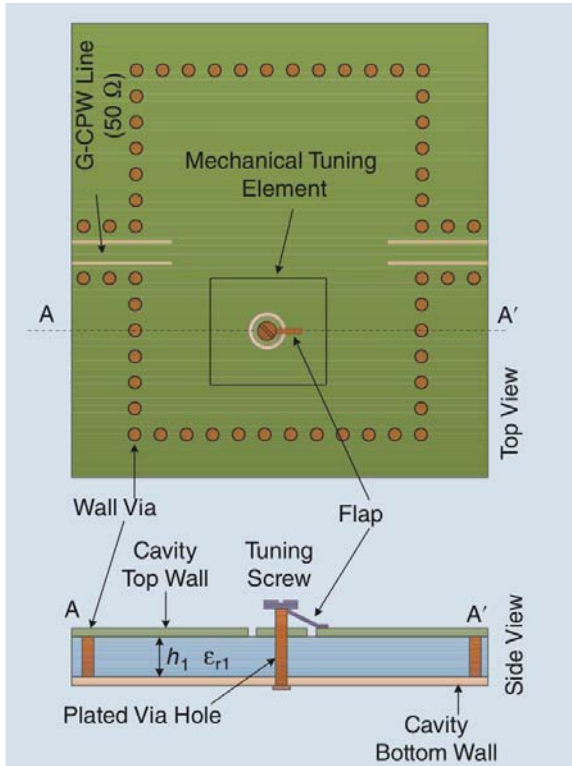

Fig. 2.5: Schematic of the tuning method of SIW structure using screwed flap adopted from [18] ©2015 IEEE.

and they are loaded with various varactor diodes. This helps to achieve a wide range of tunability which affects the quality factor of the resonator due to power consumption of various varactor diodes applied in the structure.

Since each method has drawbacks and advantages at the, it is the application that dictates which method is the most suitable option. Some methods achieve high quality factor and low loss feature, where the others provide wide tuning range. It is necessary to consider the procedure of fabricating and consequently the tuning method based on the application. Depending on the application it may be required to keep the tuning fabrication as simple as possible.

In this thesis, the combination of the two methods are employed to deliver simple but accurate tuning. The method based on floating area loaded with a varctor diode [42] and the method reported in [45] are combined. The isolated region provided by the ring gap is on the top patch and the varactor diode is loaded across the gap. By using one or two varactor diodes the power consumption is minimized. Thus, the quality factor will be high enough to allow remote interrogation using antennas. To achieve more tunability, in this study, (the first method reported in [41] was located in the vicinity of the minimum electric field) the tuning method is based on locating the varactor diode where the electric field is at its maximum. Changing the reverse bias voltage of the loaded varactor diode leads to changing the capacity of the structure (the electric field distribution also changes due to the variance of total capacity of the structure). Therefore the frequency shift occurs as expected.

2.1.2 Leakage Mechanism and Wave propagation Characteristics and Modelling Criteria

Unlike non-planar rectangular waveguides, the repeated slot array structure of substrate-integrated waveguide methodology causes leakage of the wave and more attenuation through propagation direction. A numerical study finite element method applied in [19] was performed to investigate the behaviour of the guided wave in multi-modes and analyze the complex propagation constant in terms of attenuation and modelling the frequency based on the configuration of the structure including the distance between adjacent post vias and the diameter of the conducting via. Subsequently the effective length and width are determined for SIW structures.

According to [19], only TE modes can propagate and travel along the SIW structures and transmission lines. TM modes cannot be generated and propagated through substrate-integrated waveguide structures. The dispersion characteristics of the TE modes in SIW is similar to the classic planar waveguides.

Leakage loss occurs when the electric field is not trapped between two rows of conducting post vias and part of energy propagates through the gaps between vias. It is very important to consider the leakage loss in order to maintain the high quality factor of the SIW structure. The losses are due to the leakage through the conducting vias. The behaviour of the dielectric and conductor loss is similar to the rectangular waveguide losses. The dielectric loss, represented as loss tangent, is in order of 10^{-4} [20]. The relative permittivity of most substrates used in SIW structures is in range of 2 to 14 for high frequency applications. (Reasonable results of fabricated SIW structures up to 300 GHz have been reported.) The conductor used in fabrication of parallel plates are usually copper in different thicknesses with a conductivity of $\sigma = 5 \times 10^7\ S/m$; the conductor loss is in range of few 10^{-4} Np/m.Consequently, in order to reduce the effect of the leakage loss and keep up the quality of performance the leakage loss should be less than 10^{-4} Np/m. According to [20], the dimensions of the conducting vias and their separation distance should be taken into account to satisfy the leakage loss criteria. In fact, the leakage loss coefficient should be added to attenuation constant of the propagation wave along the substrate-integrated waveguide structures [19, 20].

On the other hand, leakage loss must be greater than dielectric and conductor losses for fabrication of leaky antennas in waveguide mode as in [46]. This means that it is the application that imposes specific criteria in general. For example, at lower frequencies the substrate with a high relative permittivity could be an option in order to reduce the dimensions of the structure.

Dealing with periodic structures such as SIW, one requires to consider electromagnetic band-gap or stop-band effects. It is required to assure that there is no band-gap or stop band in the operating bandwidth. Deslandes *et al.* [20] provided criteria for the diameter of conducting post vias and periodic wave and surface impedance analysis.

In contrary, the method presented in [20] is not accurate for higher order modes because the physical discontinuities of conducting vias along propagation direction is an issue for surface currents to circulates easily. Hence, there could be a problem for analyzing higher order modes correctly by applying the the method of [20] and leakage loss.

2.2 Electric Field Sensors for High-Voltage Applications

Electric field sensors are used in a range of applications in DC, medium voltages, high voltage, and even ultra high voltage systems. There are different sensors working at low frequencies such as 60/50 Hz or even lower frequencies including few Hz in power system applications and high-voltage systems.

The importance of static electric fields and charges and consequently potential dangers caused by them could be very deadly such as explosion in charged flammable dusts. In addition, if the electric field exceeds a specific amount and get discharged abruptly without any control mechanism, it might be a dreadful situation for most of the systems (it is more dangerous to semiconductor and generally electronic devices deriving very low voltages than induced static one). Thus, it is worth measuring DC electric fields to provide a warning of probable damages.

One of the primary methods to measure static field is by using a special surface probe at standard distance from the measurand to create a capacitance between the probe and the measurand steadily. Generally the surface probe is connected to an electro-meter and by measuring the capacitance between the surface of the measurand and probe, one could get the amount of the electric field. A compensation amplifier was added to this probe to eliminate the disturbances caused by the probe unintentionally [47].

Another method of measuring DC and low frequency in the range of kVs is to apply time-varying capacitance in series with a resistance and measure the current flowing through the resistor. There are some methods to modulate capacitance including changes in distance between charged surface and a plate mechanically [47]. The other common but complicated method is to use rotating grounded chopper blade wheel which passes the proximal plate in turns [47].

The above methods are contactless and could be useful in medium and high voltage measurements, however their accuracy is limited due to difficulties of measuring the exact distance between plates and consequently measuring the capacitance. One of the digital field meters commercially available works up to 20 kV and the maximum read out distance is 4 m with reported 5 percent accuracy [47]. While other devices might require to know exact physical distance, this device can measure the distance using LEDs which improve the accuracy of the measurement.

The other common approach to measure DC electric field is electro-optical mechanism. The phenomena named electrogiration [47] is to deviate and change linear polarization of light transmitted through quartz crystal by electric field and measure the deviation in polarization corresponding to the strength of the electric field.

Another effective measurement method proposed is applying Pockels effect. This effect occurs once an electric field in direction of privileged axis causes changes in refractive indices in the other orthogonal axes. As reported in [47], some specific crystal materials including ammonium dihydrogen phosphate (ADP), potassium dihydrogen phosphate (KDP), cuprous chloride (CuCl), cadmium telluride (CdTe) and gallium arsenide (GaAs) show the Pockels effect.

Electric field detection is one of the common means of measuring voltage in general. It has been very popular in measuring voltage in high-voltage apparatus. Since the electric field distribution reveals useful information in order to maintain the apparatus in good condition. Insulation conditioning is necessary to keep high-cost power systems in proper high-quality performance. Hence, electric field sensors are used to measure both voltage and monitor insulation condition. Furthermore, the contactless measurement of the voltage could be provided by assessing the electric field surrounding the high-voltage apparatus which is highly hazardous. Due to safety issues it is favourable to monitor electric field remotely instead of contacting the sensor directly to the high/medium voltage devices.

Commonly, measuring the electric field results in a disturbance of the field which decrease the reliability of the measurement methods and devices. This problem can be mitigated by utilizing a low-loss dielectric during e-field sensor fabrication. In addition the sensor must not be grounded.

Recently, passive wireless sensors have been popular in high voltage measurements since they offer conctactless measurements. Most of these sensors are based on different types of resonators based on a tunable frequency approach. Most of the interrogation systems proposed to read out the measurements remotely are suitable slow-varying steady state measurand. Some sensors that have been proposed in different studies for high voltage applications will be covered in the following pages and their advantages and drawbacks will be discussed in terms of operating frequencies, tunability, capability of passive operation, and their remote readout distance.

2.2.1 Sensors Based on Micro-Electro-Mechanical Systems (MEMS)

These types of sensors are able to measure both DC and AC electric fields. Their complicated fabrication procedure is a main drawback of these sensors. It is required to connect these sensors directly to the interrogation system, Therefore; they are not very good candidates for high voltage measurements. Additionally, the elements used in fabricating MEMS sensors require biasing and can not operate without a power supply, and hence, they are not passive [48–52].

The proposed sensors in [48–50] are utilized in vicinity of the high voltage apparatus and industrial applications. The thermal actuators are used in presented sensors [48–50]. Furthermore the induced electric field results in thermal deviation and consequently in physical shutters' motions and laser beam defraction and capacitive monitoring could be applied to detect them. They cover a wide dynamic range from 42 V/m reported up to 500 kV/m.

2.2.2 Wireless Capacitive Sensors

The method discussed in [53] and [54] measure the root square mean (RMS) of the voltage to the medium or high voltage apparatus by direct connection. The self-calibration method is also provided for the proposed sensor. The accuracy of the sensors is up to 5 percent for almost 35 kV. The calibration for different distances to ground are also provided and the collected current data is read by an interrogation system using an antenna. The main drawback of this method is that one can only measure the voltage RMS and the proposed sensors are not contactless.

2.2.3 Electrostatic Probes

As reported in [55], there are different contactless probes employed in medium or high voltage application. The probes are utilized to determine the range of the voltage. These contactless probes are active devices using batteries and they are portable in order to use them on-site for monitoring applications. Some of the contactless electrostatic probes are used to monitor electrical isolation of the apparatus by sensing the presence of the voltage [56], [57].

Another approach discussed in [56] and [57] utilize varactors to derive the variations in the voltage using the induced electric field. Varactors employed in [56] and [57] are variable capacitors as a function of the voltage.

A separation distance from the voltage source is required in order to provide grounding connection that is required for this type of electrostatic probe. Thus, the distance from the vicinity will add the coupling capacitance and will disturb the measurements which needs to be considered.

2.2.4 Sensors Based on Intermodulation

The intermodulation method is based on sending two signals with different but close frequencies and receive the signal with the intermodulated frequency. This method enhances the performance and the interrogation distance since the difference between emitted and received signals decreases the interference [58–60].

2.3 Interrogation Systems

Recent advances in the development of wireless passive sensors have expanded their industrial applications [1–5]. Their advantage of being wireless is a key factor to employ them in situations where human contact is not favourable [6–8]. The interrogation of the passive sensors are done by remote techniques. Interrogation systems are employed that are based on either near-field coupling [5], [12] or radiative back scattering [13–15].

Near-field detection systems are more suitable for the measurement of low-frequency signals, but the interrogation distance is fairly short. On the other hand, interrogation systems that use antennas can measure high-frequency signals with a larger distance of interrogation.

Most existing passive, wireless sensors are usually employed for quasi-static measurands (*e.g.* humidity, pressure, temperature). They are not able to capture wide-band time-varying measurands. A few of these interrogation techniques are presented briefly in the following sections.

2.3.1 Near-Field Coupling Interrogation

Near-field inductive or capacitive interrogation is utilized to derive the resonance frequency or changes in impedance [7], [61]. The read-out distance is relatively less than the interrogation based on antennas and accordingly the reported quality factor is low. As presented in [6] and [13], mostly these sensors are working in low frequency (LF) to high frequency (HF) bands.The sensors proposed earlier were easy-to-fabricate structures and small in size as well. The drawback of these sensor was their very short read-out interrogation distance which dropped by a factor of $\frac{1}{R^6}$ where R is the distance from interrogation system [5, 12, 15]. Recently, novel high frequency techniques have been proposed to fabricate these types of sensors with longer interrogation distances [62].

2.3.2 Interrogations based on Radiative Back Scattering

The proposed interrogation method in [6], [18], [63] is based on sending pulses of RF signals and receiving the ring back signals of the resonator-based sensor. The frequencies of ring back pulses are derived by the detector applying peak detection method.

Frequency counting technique is described in [62] to derive the resonance frequency of sensors. This method allows to observe fast variations of the resonance frequency and is able to be employed for non-stationary measurands and has direct contact to the sensor and analyzing the variations in the voltage or current.

2.3.2.1 Interrogation System Employed in This Study

The interrogation proposed in [11] is capable of capturing the time-varying measurands. Most of the existing interrogation system are not able to obtain the measurand's changes in time. In this study, the interrogation system discussed in [11] is utilized. The system is based on sending pulses of RF signals to the sensor and receive the ring back signals re-emitted by the sensor. By deriving changes in the resonance frequency, one can find the corresponding electric field related to the resonance frequency. The interrogation distance is less than 60 cm practically but can be improved as would be its theoretical value a few meters. In addition, the samples are recorded at a rate of few MHz and the interrogation system is capable of monitoring sensors simultaneously. The interrogation system is able to determine the changes in the measurand in the range of ms practically.

2.4 Proposed SIW Resonator-Based E-Field Sensor

The proposed sensor consists of a resonator designed and fabricated using substrate-integrated waveguide (SIW) technology. The SIW resonator is coupled with a microstrip transmission line. The sensor is capable of providing tunable resonance frequency. a shift in resonance frequency is a function of an external electric field. A tuning method based on a varactor diode is designed on the patch conductor of the resonator. An isolated gap is designed on the patch conductor and the varactors are placed across the gap. The varactors are voltage-controlled capacitors. The external electric field is capable of being coupled to the isolated gap and induces voltage over the terminals of the varactors resulting in a shift in resonance frequency.

The proposed SIW sensor is passive which means there is no need to batteries and wireless which means it is capable of measuring electric field remotely. Most of the existing sensors are not passive and wireless at the same time. On the other hand, the existing wireless passive resonator-based sensors generally have less tunability and quality factor. The proposed sensor achieves wider range of resonance frequency shift than the sensor reported in [11].

Finally, the proposed SIW sensor has the following advantages:

- The proposed sensor is passive which means there is no need to batteries, and therefore it is maintenance-free.
- The proposed sensor is wireless which means it is capable of measuring remotely.
- The proposed sensor is relatively small and light-weight compared to the existing e-field sensors.
- The fabrication procedure is relatively inexpensive and the sensor is capable of being available commercially.
- The risk of flash-overs decreases since the sensor is not required to be grounded.

Chapter 3

Design of the Substrate-integrated Waveguide (SIW) Sensor

The design of the proposed sensor based on substrate-integrated waveguide (SIW) technology is presented in this chapter. The resonator-based sensors' advantages and drawbacks are also provided and their performance in the measurement of the electric field evaluated. A schematic drawing of the proposed SIW sensor is shown in Fig. 3.1. The sensor consists of an SIW resonator and a very short microstrip line that provides coupling. There is an isolated section on the patch which is coupled to the external electric field. The resonance frequency of the structure is variable due to the existence of the varactor diode across the gap on the patch. The resonance frequency change is detectable by remote interrogation using radio frequency signals transmitted to energize the sensor and obtain the damped sinusoidal signals response of the sensor. The interrogation system and the results of the fabricated sensor will be discussed in the following chapters. The COMSOL Multiphysics and HFSS Ansoft finite element simulators are used to optimize the characteristics of the design, and the results of the simulations are reported in this chapter. Finally, optimized values of the design dimensions are reported.

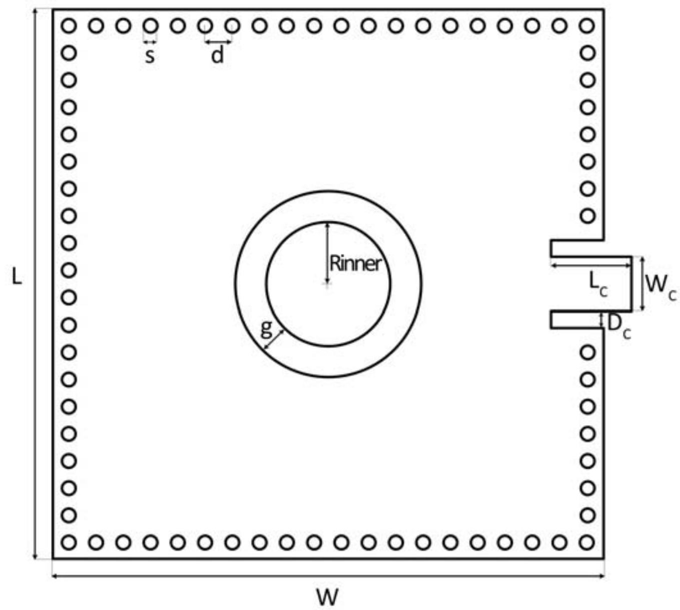

Fig. 3.1: Schematic of the proposed design for SIW resonator-based sensor.

3.1 Design Criteria

The proposed electric field sensor is based on the substrate-integrated waveguide (SIW) technology. This technology allows us to have the advantages of both classic rectangular waveguides and planar waveguides such as microstrip waveguides simultaneously on the same platform. As mentioned above, there is an isolated circular region on the patch of the resonator. This isolated region provides the capacitive coupling to the external electric field that is to be measured. A varactor diode is mounted across the gap between the isolated region and the top conductor whose capacitance is dependent on the electrical potential applied to its terminals. An external electric field induces a voltage on terminals of the varactor diode. The capacitance shift in the varactor diode results in a shift in the resonance frequency of the sensor. This structure will provide the possibility of monitoring time-varying ring back signals of the sensor using the interrogation system discussed in detail later. A microstrip with a length of less than few millimetres was designed to connect the resonator to an external antenna or a coaxial cable to energize the sensor and consequently obtain the ring back signals.

3.1.1 Substrate-Integrated Waveguide (SIW) Sensor

The designed sensor is required to satisfy design criteria in order to be employed properly to monitor electric fields. Here are the specifications taken into consideration during the design process:

1. Quality Factor: The sensor is designed to be remotely interrogated since a wireless application is highly demanded in industrial applications. A higher quality factor improves the signal-to-noise ratio received and provides more viable measurement results. SIW structures as reported in [18] provides high quality factor. Therefore, SIW resonator is a proper candidate and is chosen as a resonator-based sensor in this study. The designed SIW structure is supposed to offer a loaded-quality factor more than 200.

2. Resonance Frequency Shift: The wide range of resonance frequency shift is desirable in order to detect an external electric field with an acceptable resolution. The magnitude of an external electric field imposes a change in induced voltage which changes the capacitance of the varactor diode. As a result, a wider change occurs in the capacitance, more tunability is provided by the resonator.

3. Tuning method: As discussed in the previous chapter, there are different techniques reported to tune SIW structure. The method employed in this design is the combination of different methods to keep it relatively easy to fabricate compared to the other existing techniques. The utilized method consists of a floating area on the top conductor and a placing the varactor diode across the gap between the floating area and the rest of the patch conductor. The simplicity decreases the disturbances, increases the sensitivity of the sensor and quality factor and will be easy-to-fabricate in mass productions.

In this thesis, a varactor diode which is capacitively coupled to an external electric field or direct DC biasing is employed. The characteristic features of the varactor diode will limit the tunability and resonance frequency shift as the linear region of its response is limited.

4. Sensor Dimensions: The availability of the radio frequency (RF) components at the industrial, scientific and medical radio band (ISM Band) in range of 2.4 GHz to 2.5 GHz requires that the resonance frequency shift be limited to this band.

3.2 Design Procedure

The resonance frequency of the substrate-integrated waveguide resonator is given by [18]

$$f_{101} = \frac{c}{2\sqrt{\varepsilon_r \mu_r}} \sqrt{\left(\frac{1}{L_{eff}}\right)^2 + \left(\frac{1}{W_{eff}}\right)^2}, \tag{3.1}$$

where, as described in the previous chapter, the effective length and width of the resonator are different from the physical size of the designed resonator.

The effective length and width of the resonator are respectively given by [18]

$$L_{eff} = L - \frac{s^2}{0.95.d} + 0.1\frac{s^2}{L} \tag{3.2}$$

and

$$W_{eff} = W - \frac{s^2}{0.95.d} + 0.1\frac{s^2}{W} \tag{3.3}$$

where, s is the diameter of the vias, d is the distance between the centres of adjacent vias, and L and W are the length and width of the resonator, respectively.

Moreover, different criteria reported maintaining the reliability of the SIW performance as non-leaky structure as we need in the design of the sensor. The criteria mentioned in [18] and [20]

$$d > s \tag{3.4}$$

and

$$\frac{d}{\lambda_c} < 0.25 \tag{3.5}$$

where, s is the diameter of the vias, d is the distance between the centres of adjacent vias, and λ_c is the effective wavelength of the resonator. Considering the criteria above the dimensions of the structure is chosen as shown in Table. 3.1.

The dimensions of the substrate is chosen in particular to model one of the most viable candidates as RT/duroid 5880 with the copper cladding of $35\,\mu$m available to be employed as the low-loss dielectric.

Here, the circuit model of the sensor is shown in Fig. 3.2. The varactor diode is modelled by a capacitance across the gap between the top conductor and the isolated circular region. The capacitance of the varactor controlled by the reverse bias voltage in parallel to a capacitance available between the isolated region itself and the other part of the patch. The biasing part of the equivalent circuit model shows a low frequency voltage source which represents an external AC electric field (*e.g.* 50/60 Hz). The wires will be added to provide the reverse bias voltage in series $R_{Bias} = 1.2M\Omega$. The gap part of the circuit model consists of the capacitance of the varactor diode in parallel to a discharge resistor (which will be placed later), $C_{isolated}$ which is the capacitance between the isolated region and the ground patch, and C_{gap} representing the capacitance between the isolated floating region and the rest of the patch (at low frequencies, the rest of patch is connected to the ground conductor by metallized post vias). The resonator part of the circuit model consists the resonator's capacitor, inductor and resistor (at high frequencies). The coupling factor between the resonator and a load (a coax cable or an antenna)as a capacitance and resistor

Table 3.1: List of the parameters and the values chosen for the first design.

Parameter	*Value* (mm)
Width of Patch	79
Length of Patch	79
Width of Ground	83
Length of Ground	83
Radius of Vias	0.5
Coupling Distance	2.8
Substrate Thickness	1.575
Cladding Thickness	0.0035
Radius of Inner Circle	17
Radius of Outer Circle	18
Length of Microstrip Tline	9.5
Width of Microstrip Tline	1.6

(C_L and R_L) can be seen in the load part of the model.

One of the practical options for varactor diode is SMV2019 by Skyworks. The capacitance-reverse bias voltage characteristic of the selected varactor diode is illustrated in Fig. 3.3. To simulate the effect of the varying capacitance of the varactor, the capacitance value sweep from 0 pF to 2.3 pF is applied in Ansoft HFSS to investigate the frequency shift due to capacitance change.

Fig. 3.4 shows the behaviour of the first design according to the change in varactor diode capacitance. By modifying the capacitance up to 1 pF, the $|S_{11}|$ on dB scale decreases dramatically, and loaded quality factor of the sensor decreases to less than 200.

In spite of the fact that the tunability of the sensor reaches a value of more than 218.2 MHz, it exceeds the ISM band limitation. Moreover, the linear response of most workable varactor diodes

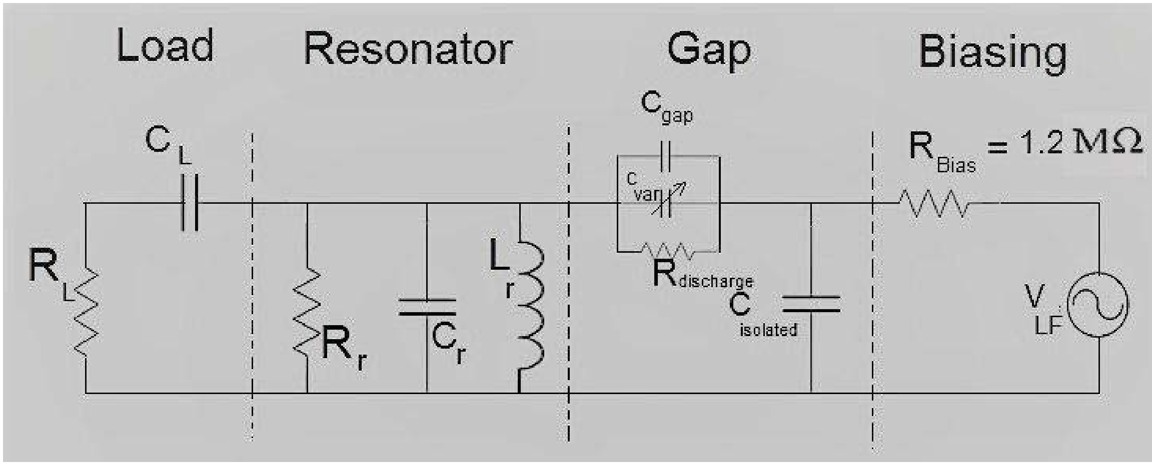

Fig. 3.2: Equivalent RF model of the SIW resonator. The RF model of the varactor is also shown in parallel with a discharge resistor.

occurs in the capacitance range more than 1 pF. Thus, it is necessary to revise the design in order not to surpass the frequency band.

The radius of the isolated circular region on the top conductor of the SIW (used to couple to the external electric field) significantly impacts the loss of the structure and consequently its quality factor. Since by changing the radius of the region, the capacitance between the region and the ground conductor and the capacitance between the region and top conductor changes. The bigger region dominates the total capacitance and hence varies the frequency drastically. In general, the Fig.3.5 provides the effect of radius factor in the design procedure. A larger radius would dominate capacitively and affect the equivalent capacitance of the gap and the varactor.

A large isolated region acts as an antenna and its radiation is not negligible due to the large value of surface current of the patch. By making the region smaller, however, the range of frequency shift covered by the same DC biasing decreases.

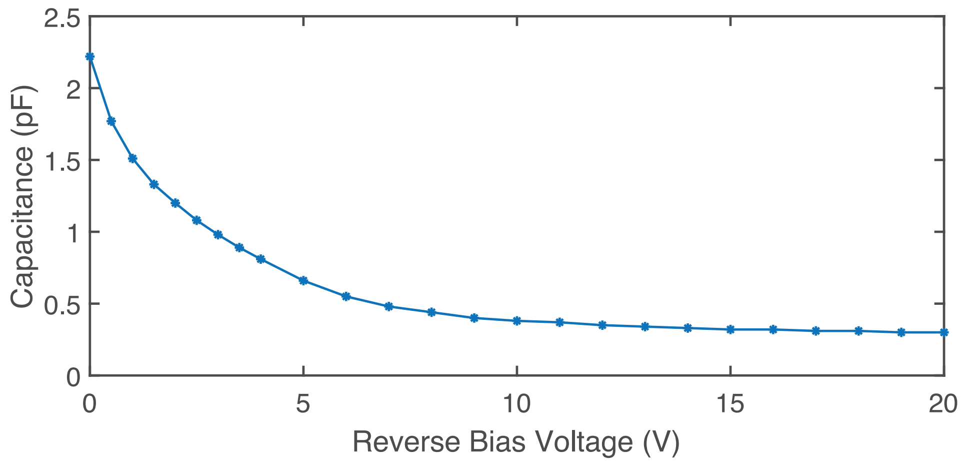

Fig. 3.3: Capacitance of varactor SMV2019 vs reverse bias voltage. The varactor shows significant sensitivity up to 5 V.

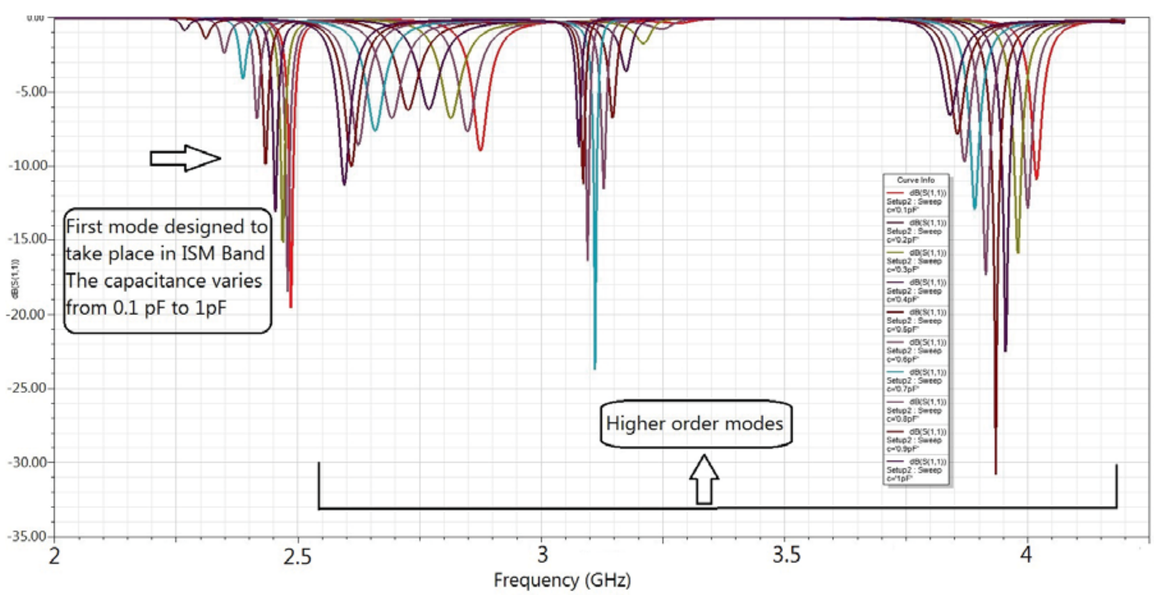

Fig. 3.4: Simulation results of $|S_{11}|$ vs resonance frequency for the first design. The capacitance sweep for modelling the varactor diode is applied.

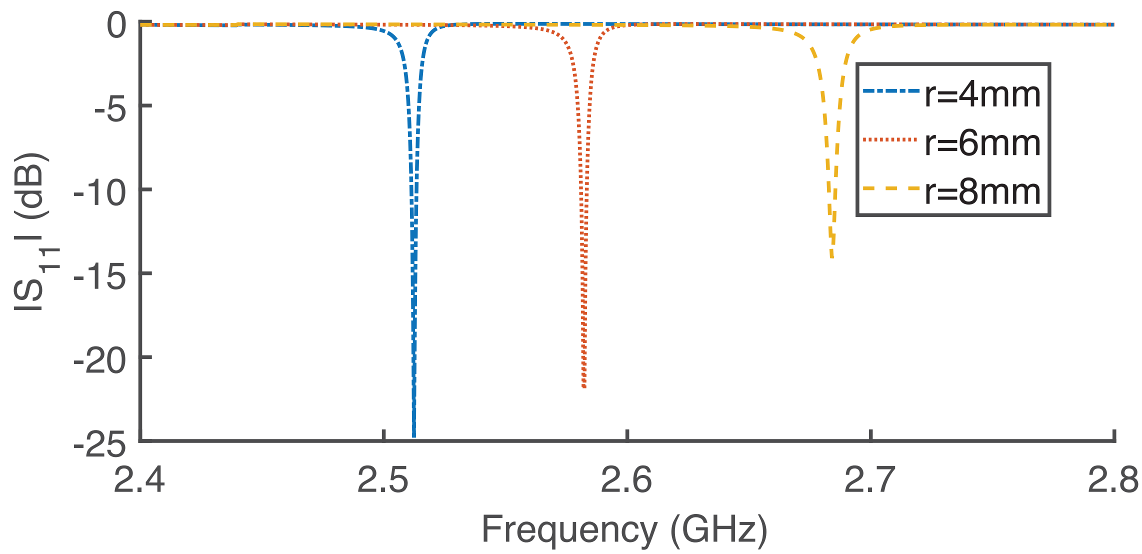

Fig. 3.5: $|S_{11}|$ simulation results of different values for inner radius of the circular isolated region.

3.2.1 Features of the Final Proposed Design

First of all, as described previously, the values of the capacitors in the circuit model are sensitive to the dimensions of the sensor. Therefore, a model of the sensor is simulated using Ansoft HFSS analysis to derive the design parameters. The list of parameters influencing the resonance frequency and frequency shift of the structure are discussed in this section to achieve the final design:

1- Radius of the isloated circular region:

As shown in Fig. 3.5, the radius of the final design is chosen to be R_{inner}=4 mm in order to minimize the radiation effect of the gap and enhance the quality-factor of the SIW resonator. The isolated region is placed where the electric field inside the resonator is maximum. By keeping the size of the isolated region small, the leakage wave out of the resonator is minimized and it will not operate as an antenna anymore. Additionally, the loss due to leakage is low enough in order to increase the quality factor to an acceptable level that is needed while the system will be interrogated remotely.

2- Width and length of the resonator:

Conversely, once a smaller value is selected for the radius of the isolated region, it will enforce smaller length and width for the sensor not to surpass the ISM band criteria. As shown in Fig. 3.2, by decreasing the radius size of the isolated region, $C_{isolated}$ drops and consequently the resonance frequency of the SIW structure decreases. In order to keep the resonance frequency in ISM Band, according to the equation 3.1 the smaller values are selected. Eventually, The width and length preferred for ground conductor both equal to 64 mm.

3- The gap between isolated region and the top conductor:

Fig. 3.6 presents the effect of the gap between the region and the patch conductor. In this case, it is worth mentioning that the finite element analysis is done without any loss and the conductors are assumed to be perfect electric conductors (PEC). As a result, the effect of loss on quality factor is neglected. Fig. 3.6 illustrates that variation in gap size causes a high deviation in resonance frequency. The other important factor is the physical dimensions of the operable varactor diodes in the desired capacitance range such as SMV2019 Skywork. According to these parameters, the gap size is selected to be 1 mm for proposed final design.

4- The coupling distance between the microstrip transmission line and the resonator:

This distance affects that how much power is delivered to the sensor and modifies the $|S_{11}|$ and the signal to noise (SNR) ratio of the damped sine wave ring back signal that is emitted by the sensor.

Fig. 3.7 is provided using the finite element analysis (Ansoft HFSS simulation result), and it reveals that not only the coupling distance (D_c) between the transmission line and the sensor will affect the quality-factor, but also it will have a slight effect on the resonance frequency as well. The reason is that the microstrip transmission line and the coupling distance is inserting the inside of the resonator somehow. This insertion causes deviation in effective length and width where the electric field inside the resonator is close to its local minimum.

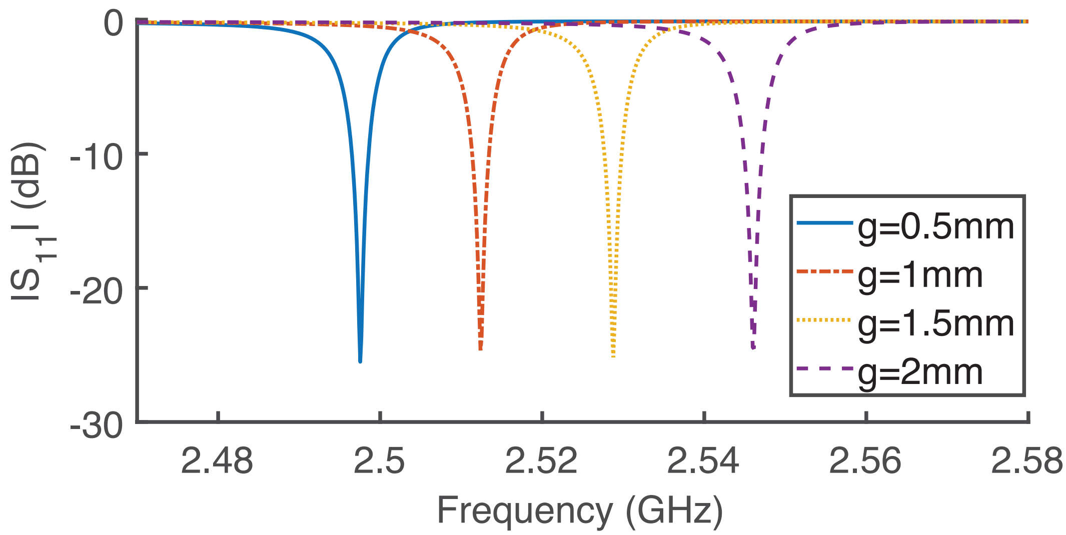

Fig. 3.6: Simulation results of $|S_{11}|$ for different values of the the isolated region gap.

5- The depth of microstrip transmission line insertion inside the cavity:

This depth causes a slight change in resonance frequency and coupling factor of the excitation where it is over-coupled or under-coupled. The effect is similar to the insertion of SMA pin insertion inside of the rectangular cavity resonator to excite it [11].

Fig. 3.8 shows the information pertinent to the depth of the microstrip line, it is concluded that an insertion depth d_{ins} of 1 mm will give a better coupling factor.

Table. 3.2 consists of all the parameters of the final proposed design as discussed above. In addition, Figs. 3.9 and 3.10 present the resonance frequency for $C = 0$ pF and, the frequency shift. The shift of the resonance frequency covers 20 MHz for a capacitance change from 2.3 pF to 0.7 pF. According to Fig. 3.3, this variation in capacitance corresponds to the 5 V change in reverse bias voltage of the varactor diode (in this region SMV2019 provides high acceptable sensitivity). The loaded quality-factors of all simulations (Figures 3.10 and 3.9) are almost 400. Therefore, the

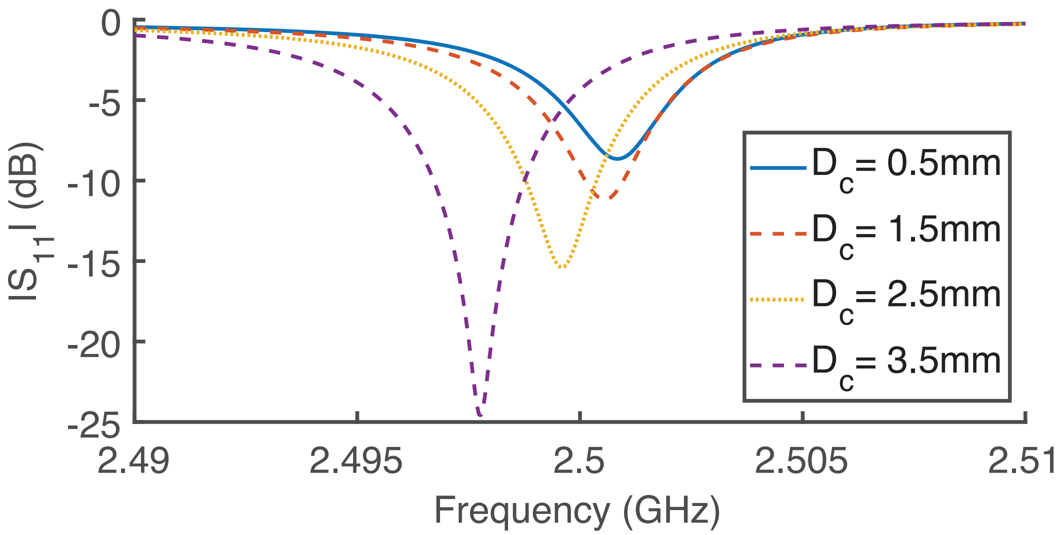

Fig. 3.7: Simulated results of $|S_{11}|$ for various values of the coupling distance (D_c).

proposed final design simulation results provide a promising candidate for the structure to fabricate.

3.3 Summary

In this chapter, the design procedure of the substrate-integrated waveguide (SIW) sensor in ISM Band was presented. The design criteria were discussed in details. Different features which affect the design were studied. Using Finite Element Method (FEM), the optimization of the features was discussed in order to design a high quality factor sensor. The optimized designed SIW sensor is capable of offering a high tunability to change the resonance frequency. Two different designs were investigated and the final design with optimized features was presented. Finally, the final design with two varactor diodes (as lumped elements) was evaluated and discussed.

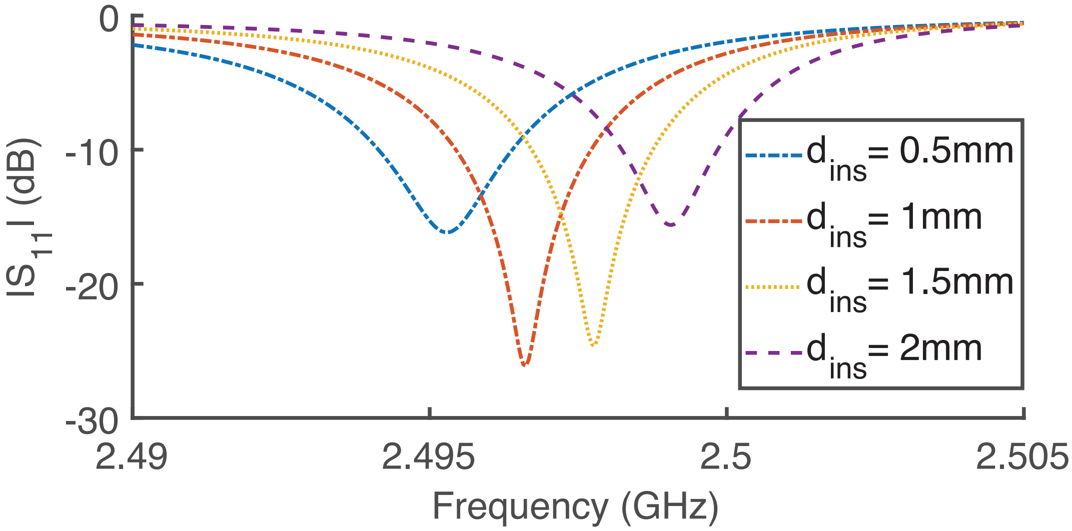

Fig. 3.8: Simulated results of $|S_{11}|$ for various values of the insertion depth of the microstrip transmission line (d_{ins}).The depth of the microstrip transmission line inserted into the resonator affects the amount of the energy delivered to the sensor.

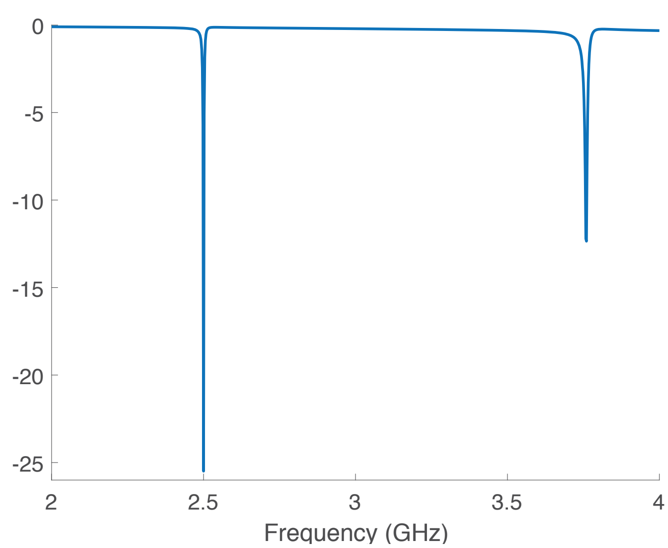

Fig. 3.9: Resonance frequency and $|S_{11}|$ of the sensor obtained from simulation for $C = 0$ pF.

Table 3.2: List of the parameters and the values chosen for the final design.

Parameter	*Value* (mm)
Width of Patch	61
Length of Patch	61
Width of Ground	64
Length of Ground	64
Radius of Vias	0.5
Coupling Distance	3.5
Substrate Thickness	1.575
Cladding Thickness	0.0035
Radius of Inner Circle	4
Radius of Outer Circle	5
Length of Microstrip Tline	3
Width of Microstrip Tline	0.5

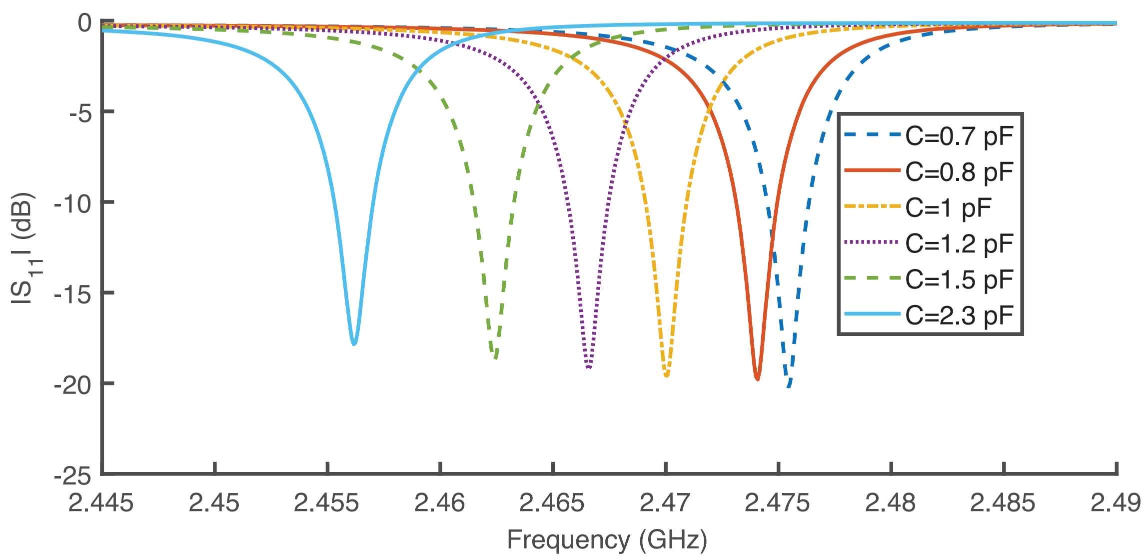

Fig. 3.10: Simulation results of $|S_{11}|$ for varying capacitance $C = 0.7$ pF up to $C = 2.3$ pF corresponding reverse bias voltage 5 V to 0 V respectively.

Chapter 4

Fabrication of SIW Sensor

The SIW sensor fabrication procedure and the measurement results are presented in this chapter. Several fabricated prototype sensors are illustrated and their response for direct DC bias applied to the terminals of the varactor diode are provided. Critical features for optimizing the sensor performance are discussed and applied to achieve the desired sensor design. The optimized sensor incorporating one varactor diode, is illustrated, fabricated, and the evaluation of its performance is discussed. In order to observe both positive and negative half cycles of AC signals, two back-to-back varactor diode are implanted across the gap and the simulation and fabrication results of this sensor are provided.

4.1 Fabrication Procedure

As there are several parameters to consider while trying to design and fabricate the resonator-based sensor, it is worth selecting and prioritizing the critical parameters in order to optimize design. Some parameters such as the size of the sensor and the radius of the circular isolated region affects the resonance frequency and its sensitivity. Moreover, the radius of the isolated region affects the resonator quality factor which can dramatically affect sensor performance. A higher quality factor is needed due to the ring back based interrogation scheme. A higher quality factor will decrease the decay of the ring back signal and the signal-to-noise ratio will be increased. This results in a high resolution of the measuring ring back signal resonance frequency. Consequently, it is a necessity to choose a substrate with low-loss features. The selected substrate is Rogers RT/duroid 5880 with copper cladding of 35 μm, a loss tangent of 0.0009, and a relative permittivity of 2.2.

The other fixed feature in the fabrication process is the varactor diode. The varactor diode chosen is Skywork SMV2019. The selected varactor diode has low resistive loss and provides high sensitivity up to 5 V of reverse bias voltage. The maximum capacitance of the SMV2019 is 2.3 pF, which is small enough to maintain the resonance frequency shift within the ISM band. As mentioned previously, the varactor is placed across the gap between the isolated ring resonator and the top conductor.

4.1.1 First Sensor Prototype

The first prototype was built based on the parameter values presented in Table. 3.1. Fig. 4.1 shows the fabricated prototype sensor. A direct DC biasing path was added using two wires in series with a 1.2 MΩ resistor. The SMA coax connector is used to connect the sensor to the Vector Network Analyzer (VNA). The VNA is used to measure the $|S_{11}|$ scattering parameter for different DC reverse bias voltages on the terminals of the varactor diode. The measured $|S_{11}|$ of the resonator before mounting the varactor diode is shown in Fig. 4.2 (a). The loaded quality factor of the resonator is around 250 which is acceptable.

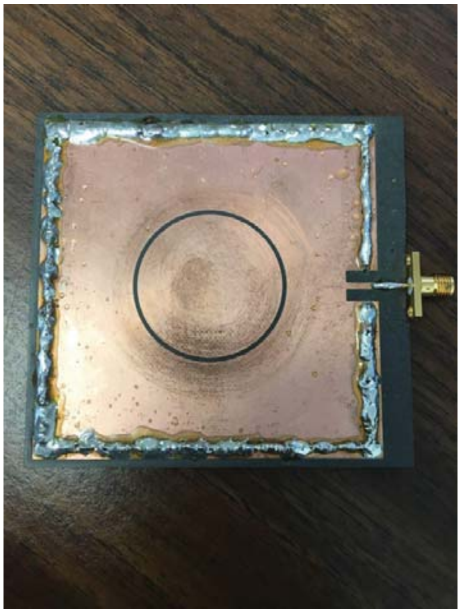

(a) Top view of the sensor.

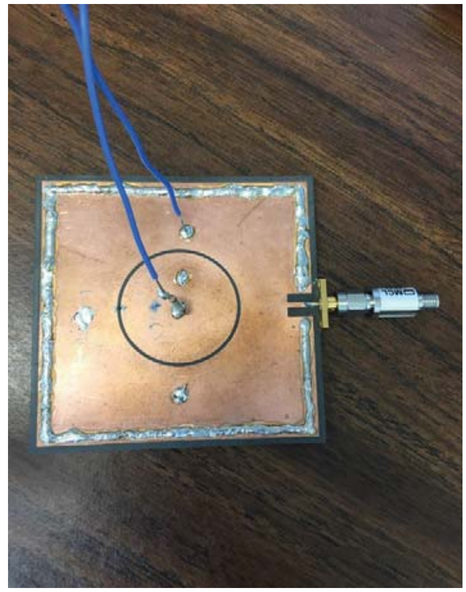

(b) Biasing wires with 1.2MΩ resistor and DC block added.

Fig. 4.1: Fabricated sensor prototype.

The measured and simulated $|S_{11}|$ parameter results are compared in Fig. 4.2 (b). There is a difference between measurement and simulation results (less than 100 MHz) but the variation is smaller for larger values of reverse bias voltage. The quality factor, as shown in Fig. 4.3 for different reverse bias voltage, is around 170 to 180. Fig. 4.3 shows that reverse bias voltage is decreased. There is a small decrease in the loaded-quality factor. A higher quality factor is needed for the interrogation method and will be discussed later.

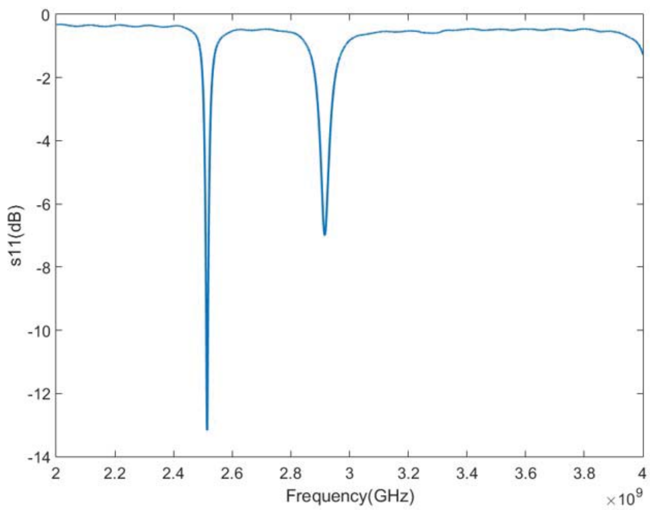

(a) Measurement of $|S_{11}|$ before mounting the varactor diode.

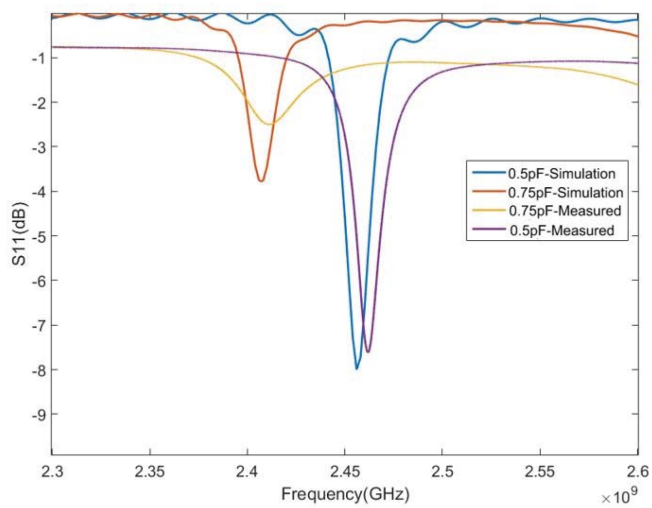

(b) Measured and simulated $|S_{11}|$ for two different capacitance values of the varactor, corresponding to reverse bias voltage of 4 V and 7 V.

Fig. 4.2: $|S_{11}|$ measurement and simulation results for the first sensor prototype.

Note that the measurement results in Fig. 4.2 b) shown -1 dB attenuation in all frequencies. This is due to an offset in the VNA and not due to the sensor.

The S-parameter measurement results of Fig. 4.2 b) shows the sensitivity of the sensor to a large voltage change. However, applying a reverse bias voltage more than 5 V is not accurate due to the non-linear capacitance-reverse bias voltage relation (See Fig. 3.3). On the other hand, for a reverse bias voltage changing from 0 V to 3 V , the measurement results of $|S_{11}|$ scattering parameter show less coupling due to large corresponding value of capacitance.

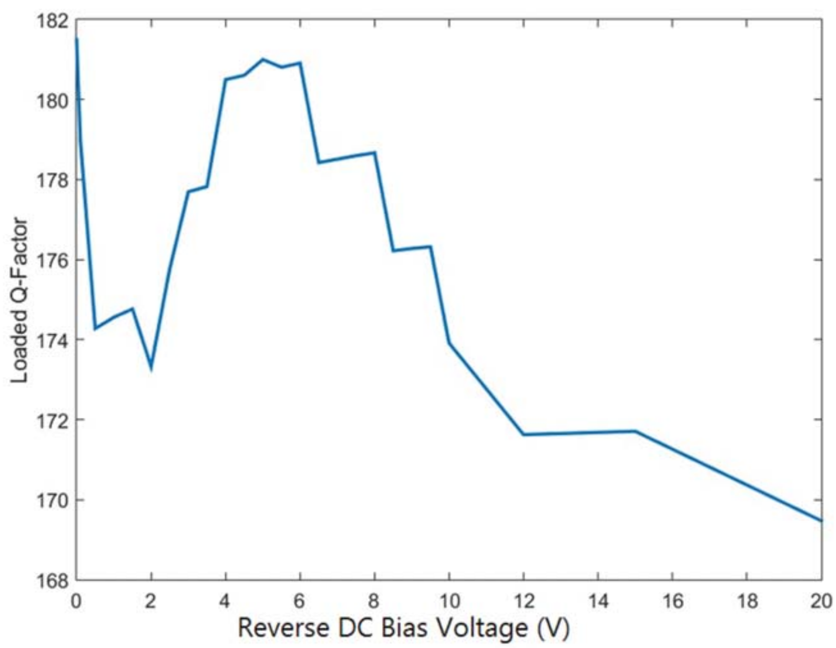

Fig. 4.3: Loaded Q-factor vs reverse DC bias voltage. Q decreases for higher values of reverse bias voltage.

4.1.2 Second Sensor Prototype with One-Varactor Implementation

As discussed in the previous chapter, a smaller radius of the isolated region enhances the quality factor and reduces the loss. Other minor features such as gap distance and depth of the coupling transmission line insertion, etc. also affect the quality factor. Their effects were discussed in Chapter 3 in detail. Accordingly, Table. 3.2 presents the final design parameter values. A Finite Element Method (FEM) software package was used (Ansoft HFSS) to model the resonator and incorporates a lumped element across the gap to act as the capacitance of the varactor diode. This is a function of the reverse bias voltage applied on its terminals. According to Fig. 3.3, to achieve a linear relationship between the reverse bias voltage and the varactor's capacitance, the maximum reverse voltage is limited to 5 V. A 1.2 MΩ resistor is also added when using direct DC biasing. The direct DC biasing mimics an external electric field. Figure 4.4 shows the fabricated SIW sensor with one-varactor implementation.

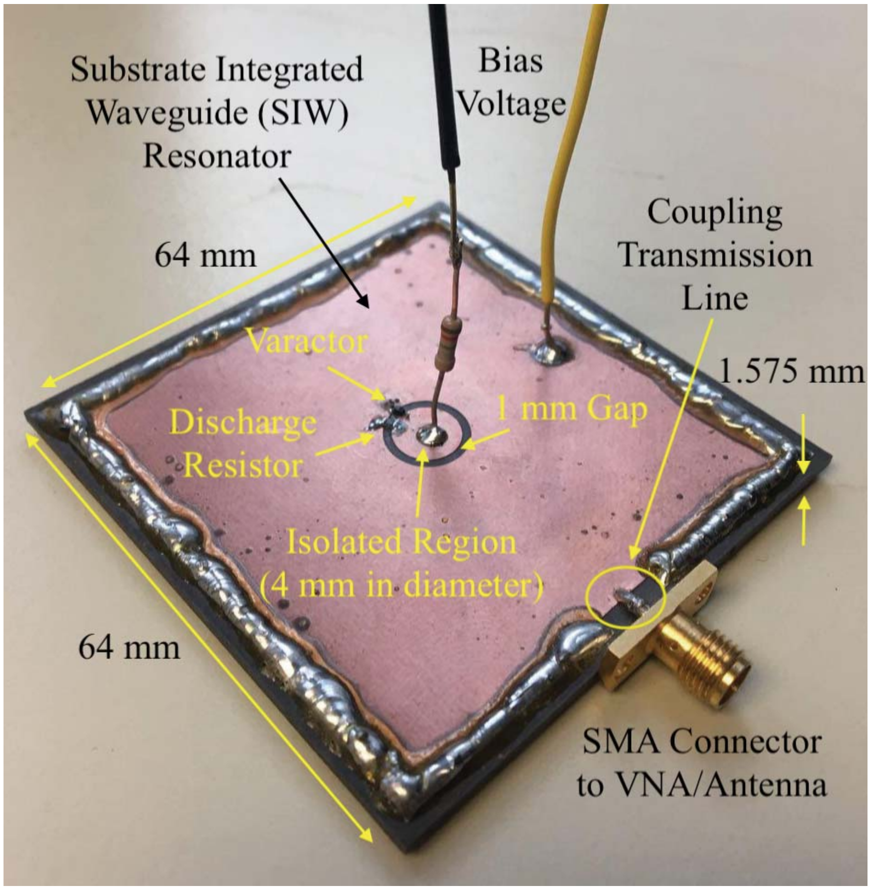

Fig. 4.4: Photo of the SIW resonator loaded with one varactor diode in parallel with a discharge resistor. The bias voltage is only applied for the evaluation of the sensor.

The simulation and measurement results are shown in Fig. 4.5. Note that Fig. 3.5 shows that a smaller circular isolated region will deliver a bigger resonance frequency shift. The shift of resonance frequency vs reverse DC bias voltage applied to the terminals of the varactor is given in Fig. 4.6 and Table. 4.1. It shows that a frequency shift of 33 MHz is achieved for a reverse bias voltage of 0 V to 5 V.

The Fig. 4.5 shows that there is a difference between measured and simulated S-parameters. The measured resonance frequency varies from $2,460$MHz to $2,494$MHz and shows higher sensitivity than the simulated results.

Table 4.1: Shift of resonance frequency vs DC reverse bias voltage applied to the varactor.

DC Bias (V)	0	1	2	3	4	5
Freq. (GHz)	2.460	2.478	2.483	2.487	2.490	2.493

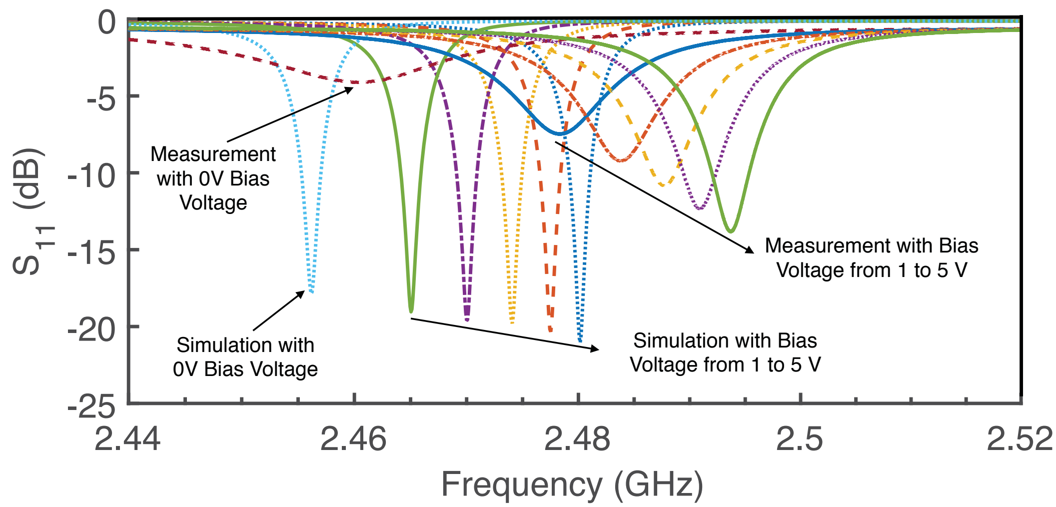

Fig. 4.5: Comparison of S-parameter of measurement vs simulation results for different reverse bias voltage (0 - 5 V).

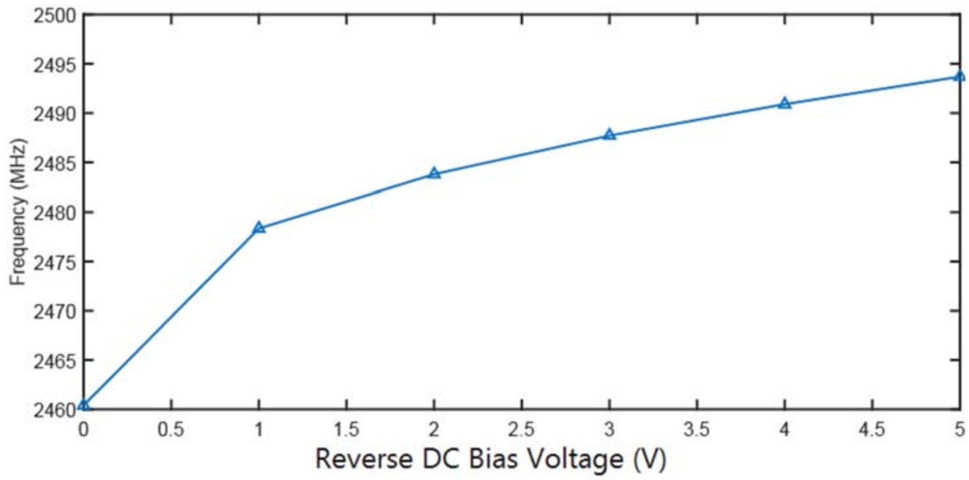

Fig. 4.6: Resonance frequency vs reverse DC bias voltage (0 to 5 V) showing a near linear behaviour from 1 - 5 V.

4.1.3 Third Sensor Prototype with Two-Varactor Implementation

An external AC electric field has negative and positive cycles and it is needed to observe both. To solve this problem, two varactor diodes in back-to-back position are implemented across the isolated region gap.

Additionally, due to the capacitance behaviour of the varactors, there has to be a discharge path. The resistor is chosen so that the impedance is dominated by the varactor at 2.5 GHz.

The fabricated sensor is shown in Fig. 4.7 without the direct DC bias wires. The sensor is analyzed using a VNA and the magnitude of the S_{11} is reported in Fig. 4.8. (a). The loaded quality factor of the sensor is 280 which is acceptable. The resonance frequency of the sensor is 2519.53 MHz. Fig. 4.8. (a) is the scattering parameters of the fabricated sensor before adding any varactor diodes or direct DC biasing wires and discharge resistor.

Fig. 4.8. (b) is the sensor measurement after implementation of varactor diodes and discharge

(a) Top view of the fabricated sensor.

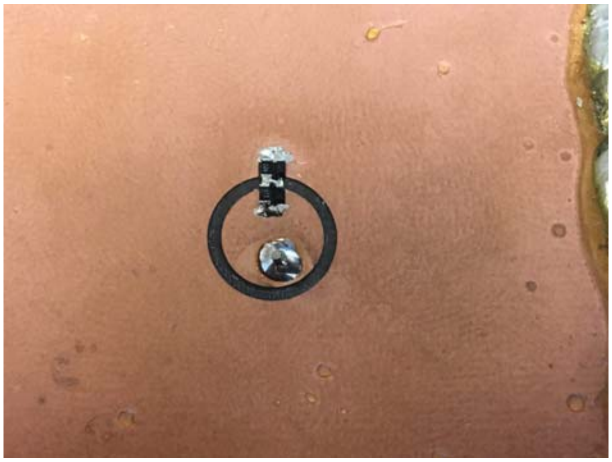

(b) The implemented varactors and discharge resistors.

Fig. 4.7: A photo of the two-varactor-loaded fabricated sensor. Varactor diodes (SMV2019) and two SMD thick film resistors ($R = 475\ \mathrm{M\Omega}$) in parallel with each varactor diode to provide a discharge path.

resistors. No DC bias is applied to the varactor diodes. The red line demonstrates the effects adding the DC biasing wires with a 1.2 MΩ series resistor through the direct biasing path. There is a 0.7 MHz difference between the measurements of resonance frequency after adding the wires. This is negligible in this application and the sensor can be calibrated using this configuration.

Figure 4.9 is the results of measurements of $|S_{11}|$ for the fabricated two-varactor-loaded sensor for DC biasing changes from 0 V to 5 V. Measurement results from Fig.4.9) are extracted and tabulated in Table. 4.2. The fabricated sensor has a tuning range of 12.95 MHz for an applied reverse bias voltage of 0 V to 5 V.

Figure 4.10 shows the measured $|S_{11}|$ of the sensor when the DC bias goes up to 14 V. Fig. 4.11 is extracted from Fig. 4.10 and shows the resonance frequency shift vs DC reverse bias voltage. The sensitivity of the sensor is high until the reverse voltage reaches 8V. Therefore, the resonance frequency varies from 2472.6 MHz to 2491.05 MHz. This covers a wide range of 18.45 MHz.

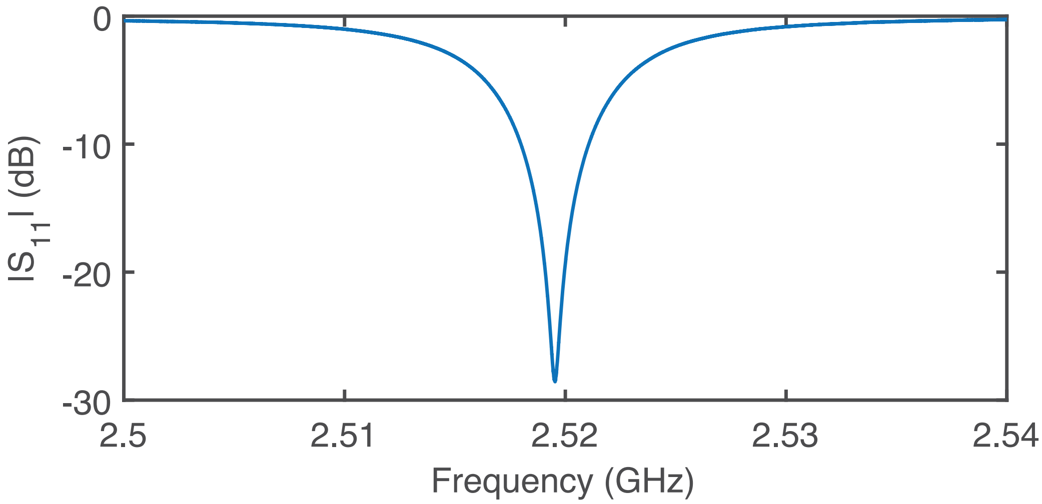

(a) Before adding varactor diodes and discharge resistors.

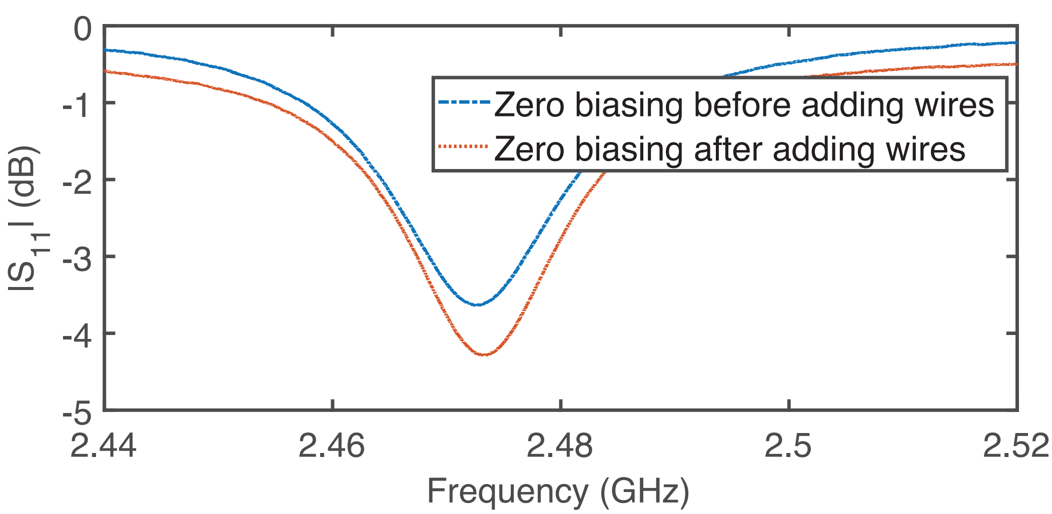

(b) After adding varactors and DC biasing wires and 1.2 MΩ series resistor.

Fig. 4.8: Measurement results of the fabricated sensor implemented with two varactors.

Table 4.2: Shift of resonance frequency vs DC reverse bias voltage applied to the varactor (data obtained from Fig. 4.9).

DC Bias (V)	0	1	2	3	4	5
Freq. (MHz)	2472.3	2474.2	2478.3	2480.55	2483	2485.25

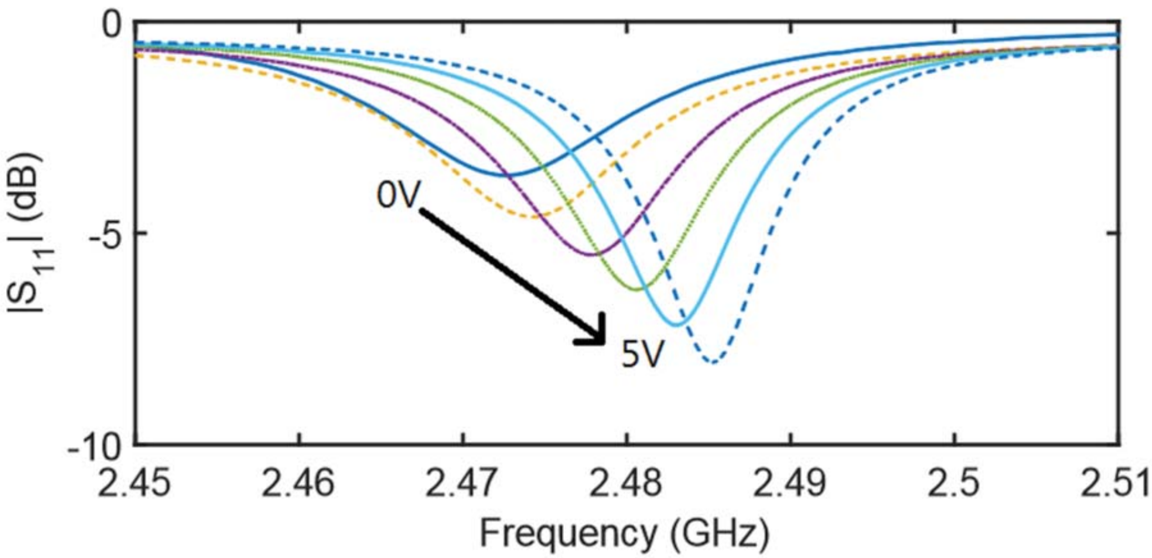

Fig. 4.9: Measurement results of $|S_{11}|$ for the final fabricated sensor while reverse bias voltage varies from 0 V to 5 V in 1 V steps.

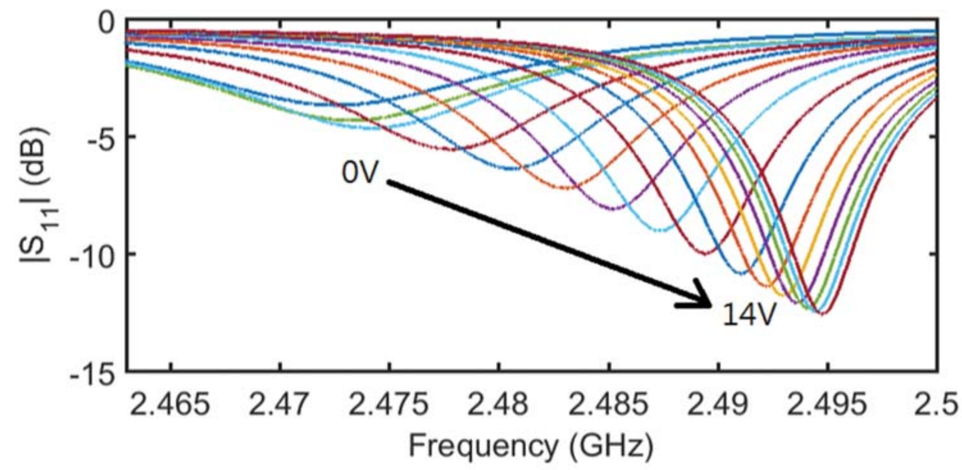

Fig. 4.10: Measured $|S_{11}|$ results for the final fabricated sensor with two-varactors implementation. The reverse bias voltages changes from 0 V to 14 V in 1 V steps.

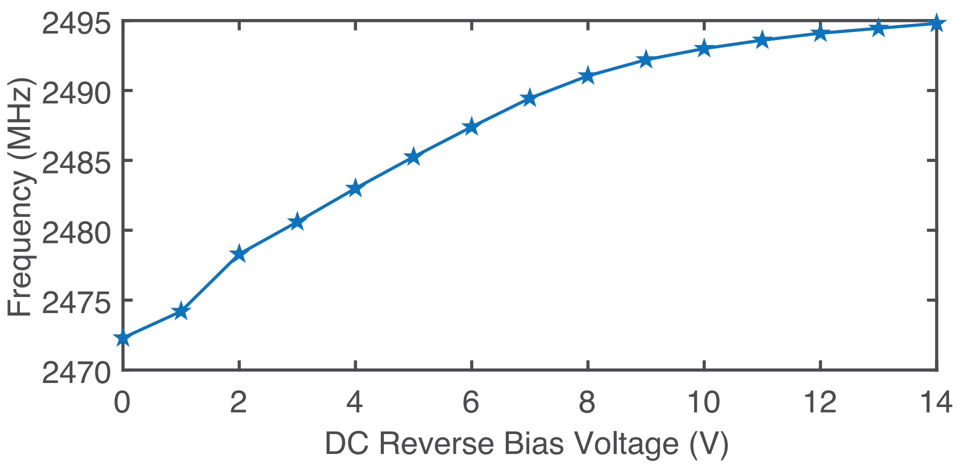

Fig. 4.11: Resonance Frequency vs DC reverse bias voltage. The fabricated sensor loaded with two varactor diodes shows a high sensitivity up to 8 V and the resonance frequency-reverse bias voltage relation provides an acceptable near-linear slope.

4.2 Summary

In this chapter, the fabrication procedure of the sensor was presented. The sensor is built based on the substrate-integrated waveguide (SIW) method. The substrate, Rogers RT/duroid 5880 with copper cladding of 35 μm, a loss tangent of 0.0009, and a relative permittivity of 2.2 is utilized. A microstrip transmission line will be used to couple the resonator to an antenna to receive/transmit signals. The resonance frequency of the cavity changes with variations in the capacitance of the varactor diode. The sensor is fabricated and tested to operate in the frequency band 2.4 GHz to 2.5 GHz (ISM Band). Important features for acceptable interrogation are high quality factor of the resonator and a large tunability in the resonance frequency, corresponding to a change in the varactor's DC reverse bias voltage. The measured sensitivity for (0 - 8 V) reverse bias voltage is approximately 2.25 MHz/V.

Chapter 5

Interrogator-Sensor Test and Characterization

In this chapter, the interrogator is described and its performance with the SIW sensor is characterized. The interrogation system is capable of observing time-varying ring back signals and is based on the approach in [11]. The presented interrogator sends a pulsed radio frequency (RF) signal to the sensor via a coax cable (in this study) or an antenna and receives a ring back signal emitted from the sensor. The ring back signal is utilized to derive the resonance frequency of the sensor which is modulated by an external electric field. Thus, a change in resonance frequency of the sensor is related to the instantaneous external electric field.

The frequency response and timing behaviour of the interrogation method is briefly provided in this chapter. The frequency domain analysis approach, to determine the time-varying response is given using the Fourier Transform method.

5.1 Interrogator-Sensor Experimental Setup

Most existing interrogation systems which are capable of operating remotely are designed to observe stationary measurands [6, 14, 63]. Since the external AC electric field we wish to measure is time-varying, the method presented in [11, 62] is employed to sample the sensor frequency with a high sampling rate. The method is based on transmitting pulsed radio frequency (RF) signals to the sensor, and receiving the re-emitted ring back signals when the transmitted RF pulse is turned off.

A block-diagram of the interrogation system is provided in Fig. 5.1. The transmitted frequency of the RF source is set to a value close to the natural frequency of the sensor in order to couple energy into it. For our sensors, the RF source frequency is selected to be either 2470 MHz or 2475 MHz.

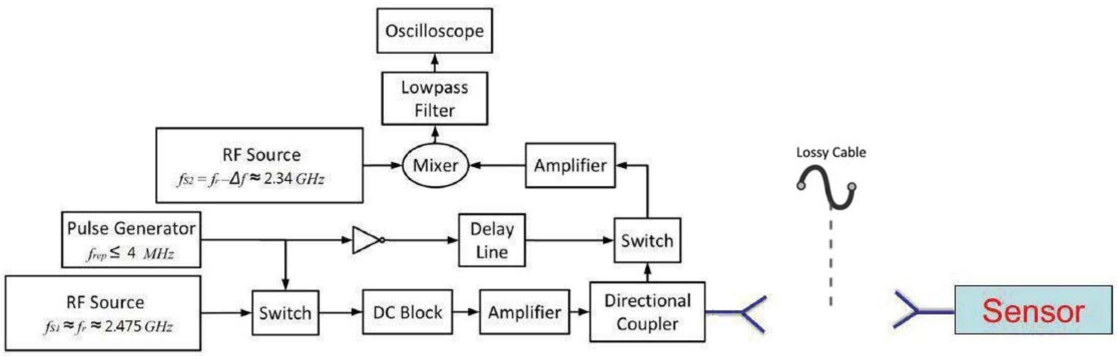

Fig. 5.1: A block diagram of the used interrogation system. A 1.2 m lossy cable with -3 dB attenuator is used to connect the interrogation system to the sensor. The lossy cable with the attenuator is modelling antennas.

There is a Transistor-to-Transistor Logic (TTL) switch through the RF path controlling the transmitted signals of the sensor. While the switch is on, the RF signal is amplified before going through a bi-directional coupler, and is then transmitted to the sensor (by antenna coupling or a coax cable). A bi-directional coupler is placed to separate transmitting and receiving paths (the coupler used adds -10 dB loss in our experiment).

When the switch is off, there is no transmitted signal, and the sensor resonates in its natural frequency. An exponentially decaying sinusoidal signal is retransmitted back to the interrogator, and reaches the coupler, and passes through the coupler path. A second switch is also added to the input of the receiver path, so that the reflected signals are removed and to impose isolation.

The received ring back signal is amplified and downconverted by a mixer, and low-pass filtered. The low pass

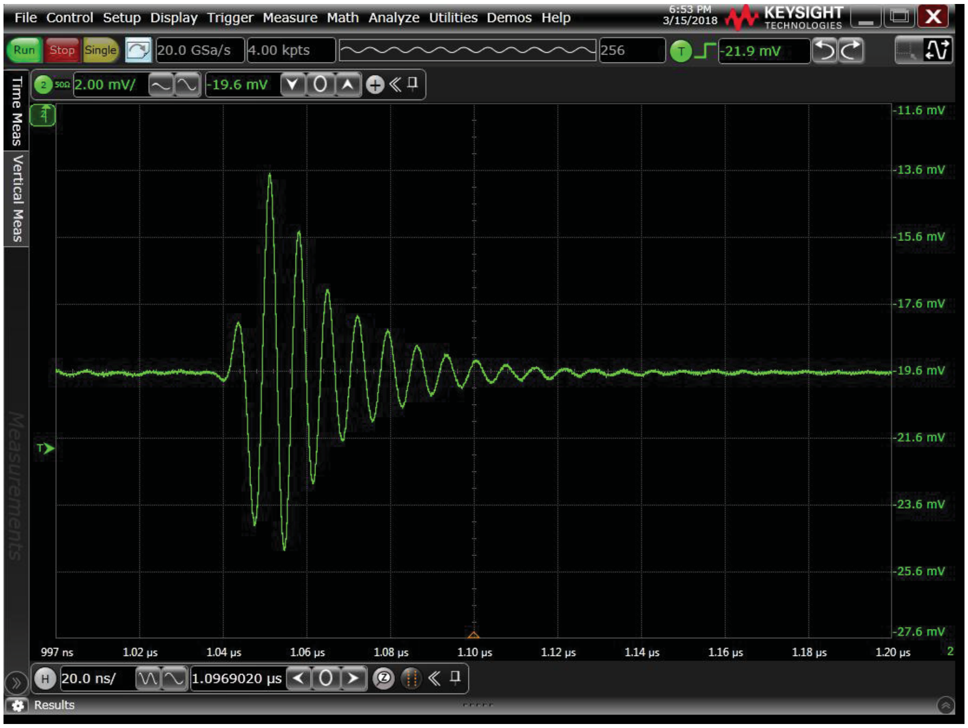

Fig. 5.2: Sample ring back signal captured using the oscilloscope.

filter reduces the high frequency noise. The local frequency of the mixer is set to 2340 MHz. Thus, the downconverted signal resonance frequency would be 120 MHz to 155 MHz for our sensor. A sample of the final downconverted, amplified and filtered signal is shown in Fig. 5.2. The duty cycle of the ring back signal is 100 ns.

A time delay is added to the receiver switch on-off timing in order to cancel the leakage signal from the bi-directional coupler and also the undesired interfering reflected signals. These are due to non-ideal components and surrounding subjects, which reflected signals when an antenna is employed.

Fig. 5.3 shows the pulsed RF transmitted signal. Fig. 5.4 shows a sample of the amplified ring back signal. It is worth mentioning that the switches have a 3 ns to 10 ns fall-time between logic on and off. The delay line also filters the effect of unwanted transients from the switches which would effect the received signal. The delay line in this study is set to the value of the 20 ns. if more delay is applied, then the amplitude of the received signal will decrease and the signal-to-noise ratio (SNR) will decrease. Therefore, there is a trade off between the delay and the quality of the received signal.

Fig. 5.3: Repetitive transmitted pulsed continuous wave (CW) signal transmitted to the sensor. The pulse repetitive rate is 1000 ns and the RF pulse duty cycle is 500 ns.

Fig. 5.4: Signal at the receiver (before the switch and downconverter) showing the ring back signal and significant interference from the RF source. The switches are set to only pass the ring back signal.

Fig. 5.5 shows the experimental setup used in this study. A laptop runs the source modules to set the RF frequencies and a fast sampling oscilloscope (Agilent DSO9254A, capable of 20 GSa/sec) is utilized to monitor the transmitted and received signals. The oscilloscope also records the final downconverted signals. In this setup, a 1.2 m cable and 3 dB attenuator is employed between the output of the coupler and the sensor in order to model a wireless path.

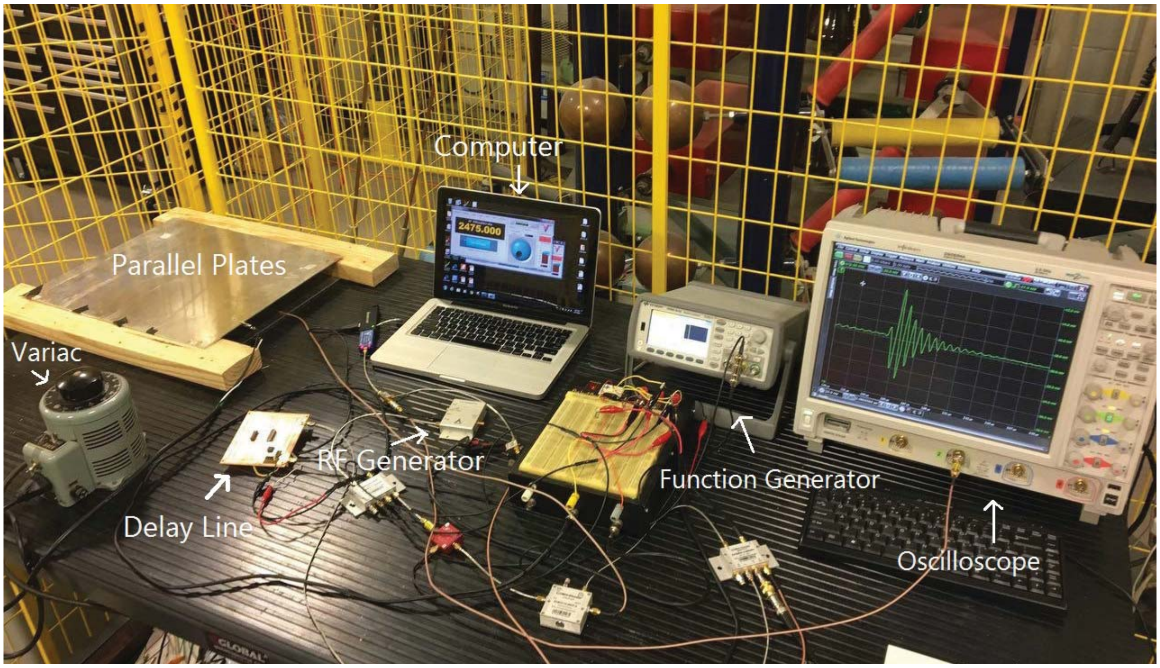

Fig. 5.5: Photo of the experimental setup. A computer controls the frequency and power of the RF sources. A function generator and the delay line provide the TTL signals to the switches. The SIW sensor is placed between the parallel plates on the left to which a high-voltage is applied. The variac controls the voltage.

To capture the multiple ring back signals the oscilloscope is set to segmented analysis mode. The recorded data from the oscilloscope is then analyzed using MATLAB in order to determine the resonance frequency of the sensor, there the data is averaged and cross-correlation is employed to improve the data. Signal averaging reduces the interrogator bandwidth, but improves the signal-to-noise ratio (SNR). A frequency domain analysis using Fast Fourier Transform (FFT) is applied to derive the resonance frequency.

5.2 Measurement Results

As a first step of this study, the AC electric field is measured by a direct bias voltage. Secondly, a 60 Hz uniform electric field, generated by applying a high voltage to a parallel plate, is measured to evaluate the performance of the sensor for measuring external electric fields.

5.2.1 Direct DC Biasing Measurement Results

5.2.1.1 Results of one varactor diode-loaded sensor

To demonstrate the performance of the sensor and interrogator, they are utilized to measure the waveform of a signal that is applied directly to the varactor's terminals (wired connection).

Here, a 50 Hz square waveform with a high level of 3 V and a low level of 1 V is applied. The signal is produced by 2-channel function generator which is also used to deliver the TTL signal to the switches. Since the sensor with one diode varactor is employed, the offset is added to avoid negative applied voltages.

The interrogation system sends a pulsed 2.472 GHz RF signal to the sensor and receives a decaying back-scattered ring back signal when the RF source turned off. The amplified and down-converted signal using an LO frequency of 2340 MHz is low-pass filtered and captured using the digital oscilloscope. A Fast Fourier Transform is then employed to determine the frequency of the ring back signal.

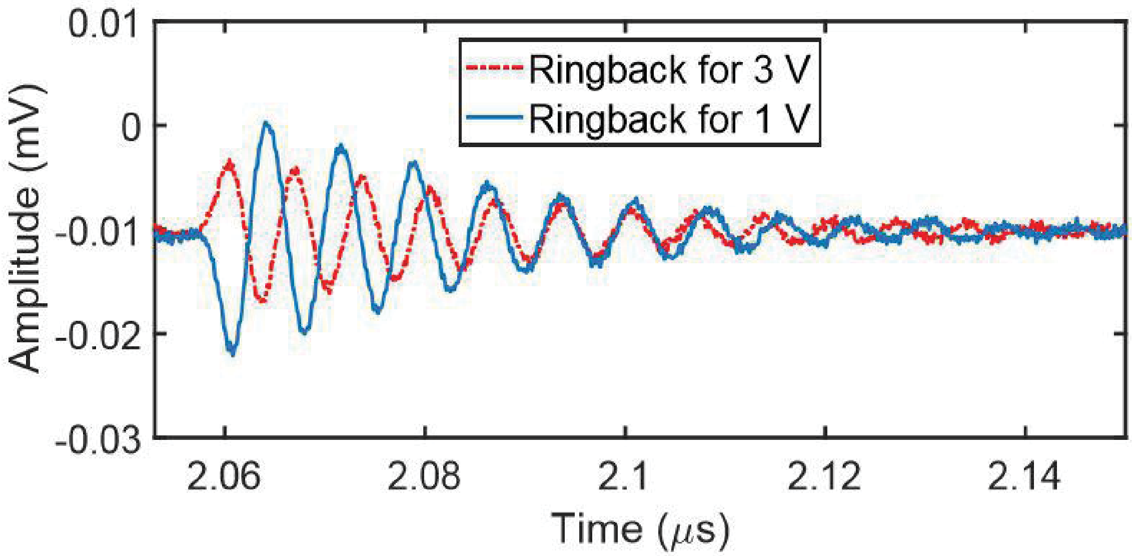

Fig. 5.6: Ring back signals for the two different levels of the AC square waveform applied directly to the varactor.

Figure 5.6 shows the down-converted ring back signals when the bias voltages of 1V and 3 V are employed.

Figure 5.8 shows the square waveform signal that is re-constructed by determining the frequency of 4,000 ring back signals. The re-constructed waveform has a peak noise of 0.0016 V. The oscilloscope is arranged to capture 2.5 GSa/s. Hence, for a 50 Hz AC square waveform, 4000 ring back sample signals are recorded. The number of ring back signals would cover two periods of the re-constructed waveform. The number of samples that can be recorded every second is limited by the quality factor of the SIW resonator-based sensor. This means that the proposed sensor can be used for measuring signals that are as fast as 4 MHz (to be discussed in details in section 5.3.1)

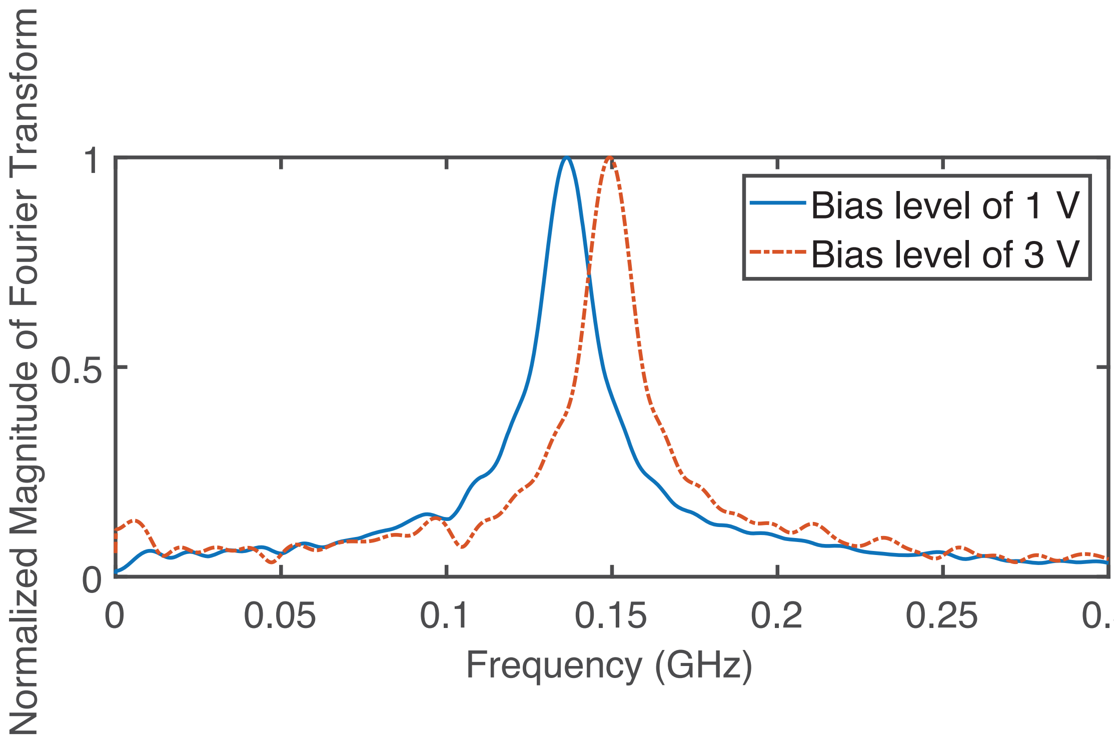

Fig. 5.7: Fast Fourier Transform of the two ring back signals showing the shift frequency due to different biasing voltages (1 V and 3 V).

Figure 5.9 shows the waveform when an AC sinusoidal at 50 Hz with high and low levels of the 3 V and 1 V reconstructed,respectively, is applied to the varactors. Here, 4000 ring back signals are captured. The deviation in the waveform is due to the fact that the cross correlation to adjust the phase shift of the ring back signals is not applied before the averaging process.

5.2.1.2 Results of two varactor diode-loaded sensor

As discussed in section 4.3.1, in order to observe negative cycles of an applied signal, two back-to-back varactor diodes are added across the gap between the circular isolated region and the top

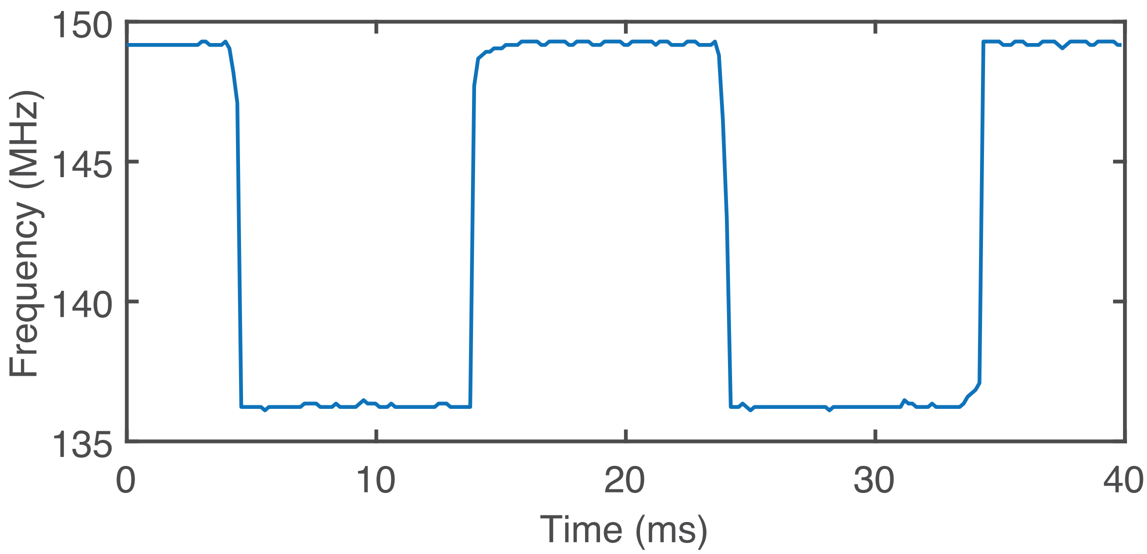

Fig. 5.8: Resonance frequency vs time obtained for a square wave signal directly applied to the sensor varactor. The AC signal is 50 Hz with minimum-maximum value 1 V and 3 V, respectively.

patch conductor and a discharge resistor in parallel with each varactor is added. The resistor value is chosen to be large enough to provide a DC discharge path.

Using a function generator, an AC 50 Hz sinusoidal signal (with 6 V peak-to-peak and no offset) and a 50 Hz square waveform (with high and low levels of 3 V and −2 V, respectively) are applied directly across the varactors. The same experimental setup is employed. The reconstructed ring back signals for the sinusoidal and square waveform are given in Fig. 5.10 and Fig. 5.11, respectively.

Since the sensor provides a rectified output, it is not possible to identify which half cycle of the sinusoidal shown in Fig. 5.10 belongs to the negative cycle. Additionally, the varactor diodes are not identical, so their voltage-capacitance characteristics are not the same, and results in different peaks for positive and negative cycles. The discharge time constant of the parallel resistor-varactors is $RC_{var} \simeq 1ms$. This reduces sharp changes in zero-crossing.

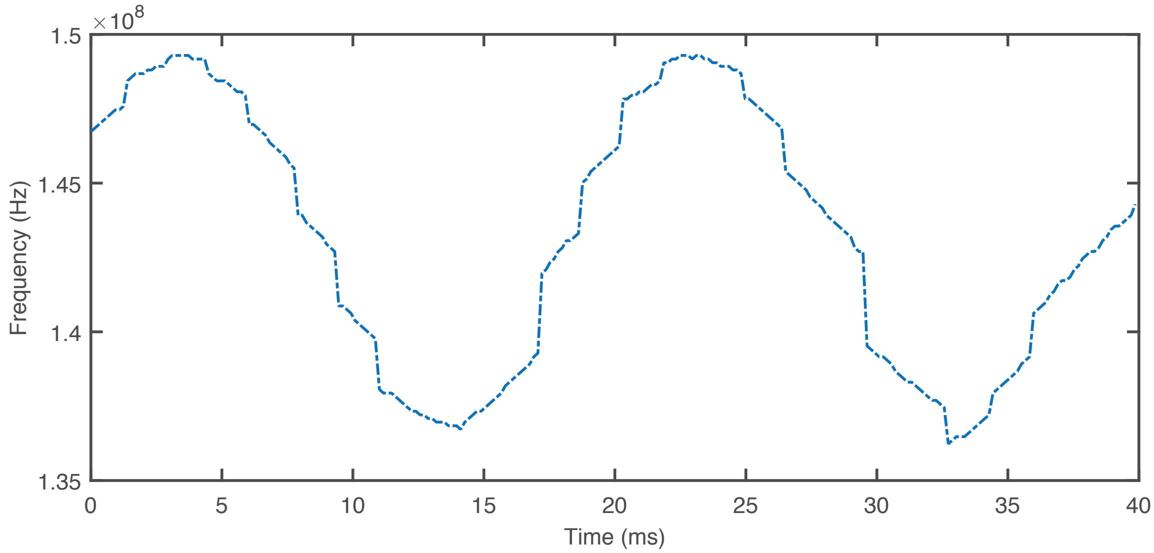

Fig. 5.9: Resonance frequency vs time for an applied sinusoidal 50 Hz signal directly to the sensor varactor. Two periods of the measured signal are shown. The cross correlation technique was not applied once this waveform was derived.

Note that the frequency shift reported in Fig. 5.10 for a maximum value of the 3 V, matches the frequency reported in Fig. 5.7.

The values of the high and low levels for reconstructed square waveform in Fig. 5.11 can easily be distinguished. The negative cycles is set to -2 V and results in a frequency shift of $\Delta f \simeq 146$ MHz. The positive cycle is set to $+3$ V and results in a value of $\Delta f \simeq 152$ MHz. In both cases the mixer as local frequency is 2340 MHz.

Here, three different approaches are used in order to derive the resonance frequency of ring back signals and accordingly reconstruct an applied waveform. Note that the above is done by applying FFT analysis on ring back signals. The first approach (method A) uses the output signals of the oscilloscope. The only employed signal processing method here is averaging to reduce the effect of the noise and enhance the signal-to-noise ratio (SNR). The Second method (method B) employs a part of the output signal of the oscilloscope in time to avoid sharp changes occurring once the sensor starts to re-emit the ring back signals. Since the different ring back signals‘ starting time is different, the third approach (method C) benefits from cross-correlation to adjust the phase shift before applying averaging to make signals start from the same point. It is concluded that applying the cross correlation is crucial before averaging the ring back signals. (See Fig. 5.9).

Fig. 5.12 and Fig. 5.13 are the reconstructed sinusoidal and square waveforms respectively when the three different ring back analysis approaches are used.

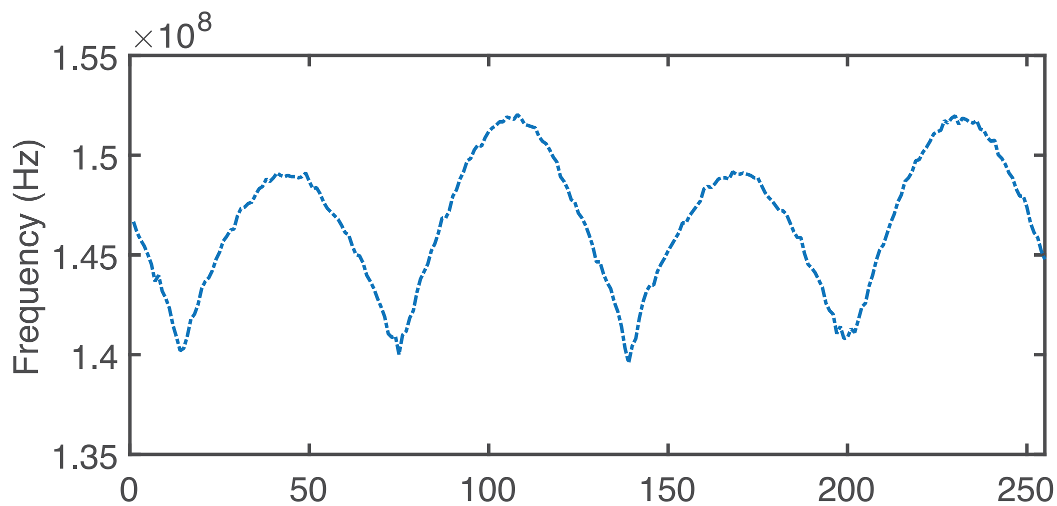

Fig. 5.10: Resonance frequency vs number of averaged ring back samples when a sinusoidal 50 Hz waveform with no offset and V_{p-p}=6 V is directly applied to the varactors ($\Delta t = 0.16$ ms between two adjacent samples which covers 40 ms in total). The reconstructed signal for both half-cycles are positive. The difference for peak values in negative and positive cycles is due to the different characteristics of the diodes used.

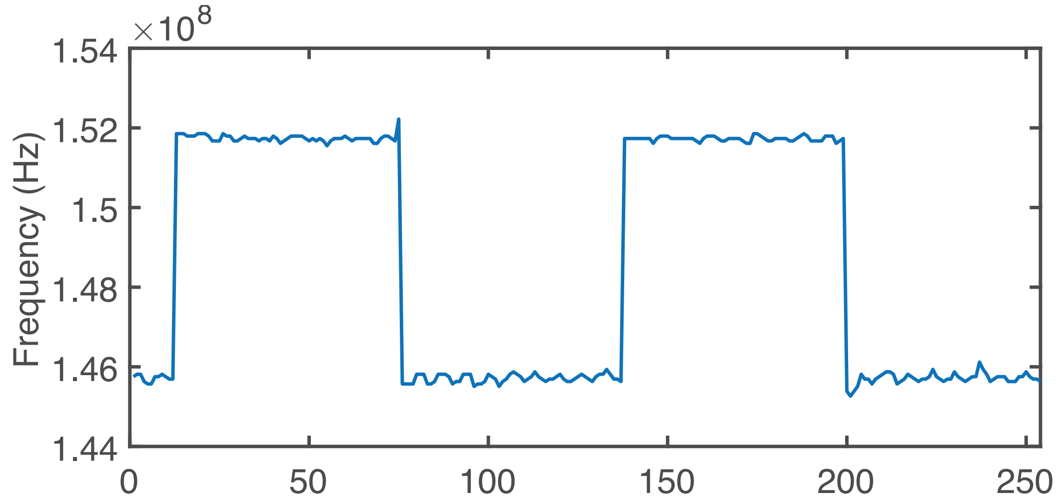

Fig. 5.11: Re-constructed 50 Hz square waveform with high and low levels of 3 V and 2 V, respectively ($\Delta t = 0.16$ ms between two adjacent samples which covers 40 ms in total).

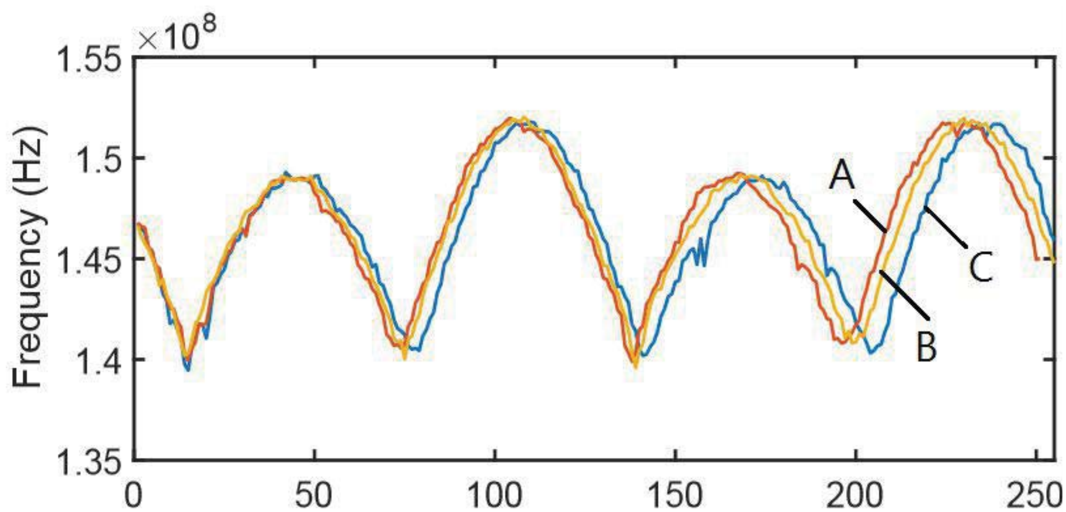

Fig. 5.12: Re-constructed 50 Hz sinusoidal signals with no offset and V_{p-p}=6 V for three different ring back analysis approaches ($\Delta t = 0.16$ ms between two adjacent samples which covers 40 ms in total).

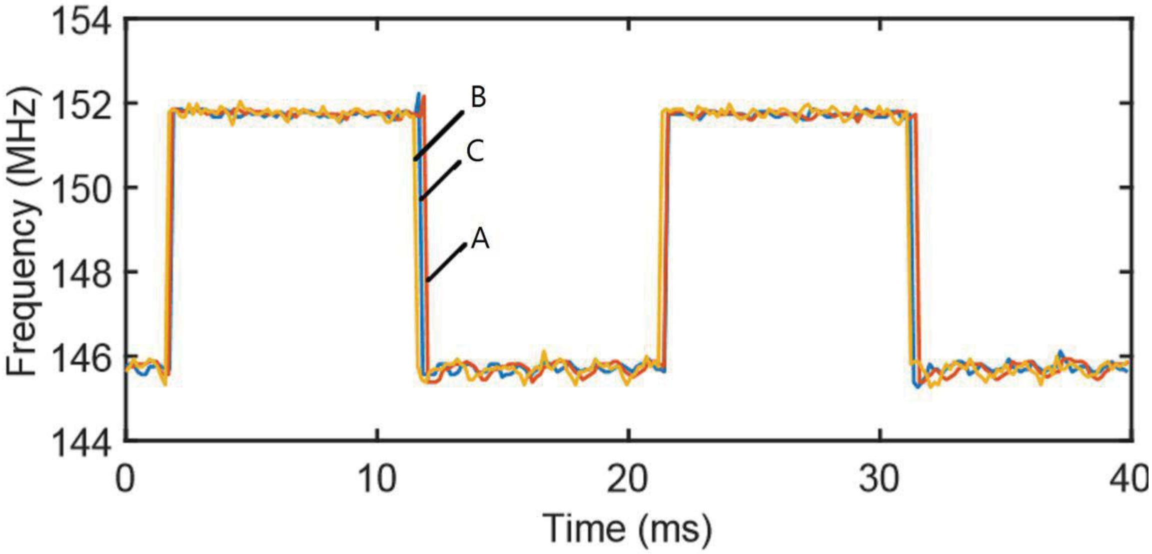

Fig. 5.13: Re-constructed 50 Hz square waveform for three different waveform analysis approaches (high and low levels of 3 V and 2 V, respectively).

5.2.2 External Electric Field Measurement

To measure the SIW sensor's response to an external electric field the sensor is placed between two energized parallel plates as shown in Fig. 5.14. A 60 Hz sinusoidal voltage is applied to the plates using a variac. The SIW resonator based sensor is located on the grounded plate and fixed in place utilizing copper tape.

The variac could apply a voltage up to 120 V_{rms}. The distance between the plates was 4cm resulting in a maximum field E_{rms}= 3 KV/m. COMSOL Multiphysics was used to determine the induced voltage across the isolated region gap of the sensor. The maximum induced voltage corresponding to the maximum field amplitude is 2.8 V, which results in a 28 MHz frequency shift (using Table. 4.1). The sensor was located in the centre of the ground plate similar, to the simulations. The direct DC Bias Voltage wires and the 1.2 $M\Omega$ illustrated in Fig. 4.4 was also removed.

Similar to the direct DC biasing analysis, the interrogation system described in the previous

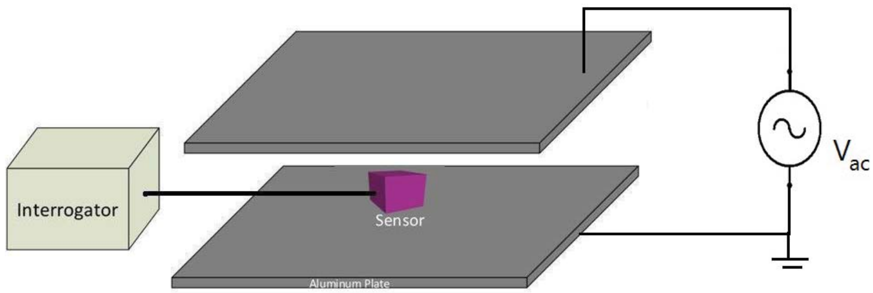

Fig. 5.14: Measured resonance frequency vs time for a $3\ KV_{rms}/m$ 50Hz AC electric field generated by two parallel plates. Slightly more than two periods of the signal are shown.

section is used to send pulses of 2.475 GHz and analyze the received ring back signals. The local frequency utilized to downconvert the ring back signals is 2.34GHz. As obtained from Fig. 4.5, with applied field the resonance frequency is 2.46 GHz and consequently the downconverted frequency would be 120 MHz.

The re-constructed AC electric field obtained by collecting the frequencies of $4,000$ ring back signals per second is shown in Fig. 5.15. Since the sensor used in this experiment includes only one varactor diode, it detects only positive cycles of the AC electric field. The measured frequency of the ring back signal in no field applied is 120 MHz as expected. the measured frequency shift is 31 MHz which corresponds to the expected frequency shift in Table. 4.1.

5.3 Interrogator-Sensor Performance Evaluation

In this section, performance evaluation of the proposed SIW sensor is discussed. Time and frequency domain analysis of the interrogator-sensor experimental setup are also provided. The accuracy and sensitivity of the measurements are quantified as well. In order to detect an external AC electric field, the dynamic frequency range of the proposed sensor is presented.

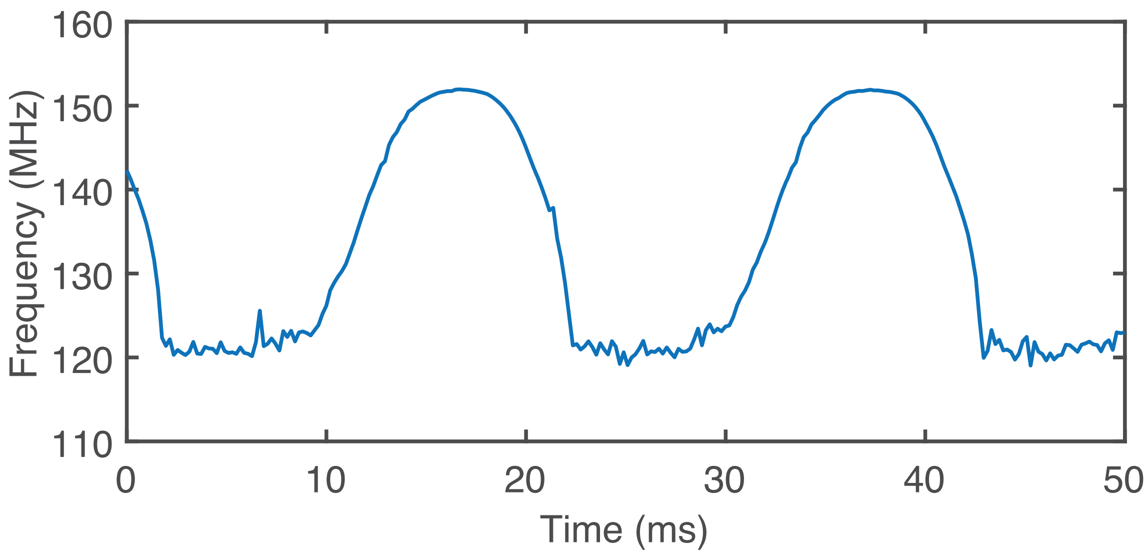

Fig. 5.15: Measured resonance frequency vs time for a $3\ KV_{rms}/m$ 50Hz AC electric field generated by two parallel plates. Slightly more than two periods of the signal are shown.

Note that the mapping is required in order to derive an external electric field from measured frequency shift using the frequency vs reverse bias voltage curve. The curve as shown in Fig. 4.11 is derived using the $|S_{11}|$ scattering parameter measurements. The finite element COMSOL Multyphysics is used to derive the electric field vs (induced) reverse bias voltage. Thus, the resonance frequency vs time which is reconstructed can be mapped to deliver the external electric field vs time.

5.3.1 Interrogation Frequency Analysis

There is an error called aliasing error which occurs when there is not enough samples per cycles to reconstruct the signal. In order to avoid this error, according to Nyquist criteria, it is required to sample at a frequency at least more than two times the frequency we are interested in. To reconstruct a sinusoidal signal to an accuracy of more than 1 percent, it is required to have more than 15 samples per cycle. Thus, for an 50/60 Hz AC electric field, a minimum sampling rate of 750/900 samples/s is required.

According to the Table 4.1, the SIW resonator loaded with one varactor can be assumed as an ideal filter operating in the range of 2460 MHz to 2493 MHz with a bandwidth of $f_{res}/Q \simeq 9.9$ MHz. For enhancing the coupling of the resonator, the RF frequency of the transmitter is set to be 2475 MHz. Therefore, the RF pulse duty cycle (T_0) is required to be 1/9.9 MHz $\simeq$ 100 ns.

As mentioned above, the transmitter sends the RF signals with $f_{transmitter} = 2475$ MHz and the sensor re-emits the ring back signals which last almost for 100 ns (see Fig. 5.2). The loaded quality factor of the resonator-based sensor can be found as

$$Q = \tau\pi f_{res} \tag{5.1}$$

In this equation, τ represents the time constant of the ring back signals (it is almost 30 ns where the amplitude of the ring back signals drop by $\frac{1}{e}$) and Q is the loaded quality factor which equals to 235.

As mentioned above, 100 ns (RF pulse duty cycle) is required to energize the sensor, and $5\tau = 150$ ns is necessary for the ring back signals to damp. Thus, the pulse repetitive rate should be as following

$$T_{rep} = 100\ ns + 150\ ns = 250\ ns \tag{5.2}$$

and then

$$f_{rep} = 1/250\ ns = 4\ MHz \tag{5.3}$$

where f_{rep} is the maximum suitable switching frequency of the interrogation system. The averaging is utilized to reduce the effect of the noise (10 samples are averaged). The averaging reduce the sampling rate to $f_{rep}/10 = 400$ kHz which is still higer than required sampling rate as 900 samples/sec for an AC 60 Hz electric field.

5.3.1.1 Electric Field Measurement Bandwidth

The sampling rate of the interrogation system limits the frequency dynamic range of the detectable AC electric field signals utilizing the proposed SIW sensor. On the other hand, the sensor itself also imposes some limitations. These two limitation factors, restrict the bandwidth independently.

It is determined that the maximum sampling rate of the interrogation system is 400 kHz after averaging (averaging rate n=10) and without averaging a rate of 4 MHz is achieved. In order to detect the sinusoidal signal with 1 percent accuracy, at least 15 samples are required. Therefore, the upper cutoff frequency for measuring the time-varying electric field using the proposed SIW sensor is 26.7 kHz and 267 kHz with and without averaging, respectively.

On the other hand, the operating frequency of the varactor diode also limits the cutoff frequency of the measurable electric field. The operating frequency of the varactor diode used in fabrication (Skywork SMV2019) is less than 1 MHz. The upper cutoff frequency imposed by the sampling rate of the interrogator (400 kHz) is less than the operating frequency of the varactor diode.

The lower cutoff frequency is limited by the minimum current of the varactor diode in reverse bias (I= 0.01 pA). Then we have

$$I = C\frac{\mathrm{dV}}{\mathrm{d}t} = C\frac{\mathrm{d}}{\mathrm{d}t}(A_V sin(\omega t)) = C \times A_V \omega(cos(\omega t)) \tag{5.4}$$

where C is the capacitance of the varactor diode, A_V represents the induced reverse bias voltage over terminals of the varactor diode and ω is the angular frequency of the external applied electric field. The maximum capacitance delivered by the SMV2019 is $C_{max} = 2.25$ pF, and assume that

$cos(\omega t) = 1$, therefore

$$C \times A_V \omega (cos(\omega t)) \geq 0.01pA \quad (5.5)$$

and

$$(2.25\ pF) \times A_V \omega \geq 0.01pA \quad (5.6)$$

which results in $A_V \omega \geq 0.0044\ A/F$, where induced voltage (A_V) over varactor's terminals varies 0 V to 5 V. As a result, the lower cutoff frequncy is in a range of few mHz.

5.3.2 Sensitivity of the Proposed Sensor

The sensitivity of the proposed SIW sensor is defined as $\Delta f_{res}/\Delta V_{induced}$ which is required to be maximized. The variation of the induced voltage over the terminals of the varactor diode from 0 V to 5 V is linearly related to the applied external electric field.

The induced voltage over the varactor's terminals is set to 2 V and the deviation of the 100 mV is applied to derive the sensitivity. The ring back signals are received in the interrogation system, downconverted using a mixer with $f_{LO} = 2340$ MHz. The derived frequencies are reported in Table. 5.1. The sensitivity can be measured using Table. 5.1 as 2.3194 kHz/mV and 6.002 kHz/mV for the sensor loaded with two varactors and the sensor loaded with one varactor, repectively. The proposed sensor with two varactors shows more sensitivity. On the other hand, the sensor loaded with one varactor offers more tunability in frequency shift (see Tables. 4.1 and 4.2).

Note that the reported (downconverted) resonance frequencies in Table. 5.1 are the average value of several derived frequencies. Thus, using the values of Tables 4.1 and 5.1, the accuracy of the measurement (using one varactor-loaded sensor) for the applied reverse bias voltage of 2 V is

Table 5.1: The induced voltage vs the downconverted frequency.

Induced Voltage (V)	1.9	2	2.1
Frequency (MHz) of the two varactor-loaded sesnor	145.877075	146.139526	146.340942
Frequency (MHz) of the one varactor-loaded sensor	140.490723	140.841675	141.751099

as following

$$1 - \left| \frac{140.85MHz - 142MHz}{142MHz} \right| = 0.9919 \tag{5.7}$$

and the measurement accuracy for two varactor-loaded sensor is as following

$$1 - \left| \frac{146.14MHz - 138.3MHz}{138.3MHz} \right| = 0.944 \tag{5.8}$$

where the one varactor-loaded sensor shows more accuracy.

5.3.3 Effect of the Environmental Temperature

The resonance frequency of the proposed resonator-based sensor is not vastly pertinent to the environmental temperature. A change in the temperature will affect the length and width of the resonator resulting in a change in resonance frequency. Thermal characteristics of the utilized substrate and cladding coppers affect the resonance frequency. The used varactor diode capacitance is also variable slightly due to the change in the temperature. The thermal coefficient of expansion in x and y directions of the used substrate (Rogers RT/Duroid 5880) are 31 and 48 ppm/°C respectively and the operable range of the substrate is $0 - 100$ °C, and the thermal coefficient of the relative permittivity (ε_r) is -125 ppm/°C (in the range of -50 $-+150$ °C). The selected varactor diode (SMV2019 Skywork) is operable in a range from -55 °C to 150 °C. Further measurements are needed to derive the resonance frequency dependency on the temperature for different reverse bias voltages over the terminals of the varactors.

Since we investigate the shift in resonance frequency in order to reconstruct an external electric field, the sensor's resonance frequency pertinence to the environmental temperature will not affect the electric field profile drastically. Another resonator-based sensor could be employed to compensate the dependence on temperature. the second sensor is utilized to gather the data to calibrate the sensor which is measuring the electric field. The variation induced due to the temperature shift could be compensated by the second temperature-sensor.

5.4 Summary

The interrogator experimental setup was presented, fabricated and utilized to evaluate the performance of the proposed SIW sensor. The interrogation system sends pulses of RF signal and receives the ring back signals re-emitted by the sensor while the transmitter is off (by a switch). The received ring back signals are downconverted by a mixer and captured using an oscilloscope. The resonance frequency of each ring back signal is derived using a frequency domain analysis (fast Fourier transform (FFT) analysis). The resonance frequency of the proposed sensor is modulated by an external electric field. Thus, a shift in the derived resonance frequency of the sensor is a function of the the corresponding external electric field. This procedure provides the reconstructed waveform of the applied external electric field.

The performance evaluation of the interrogator-sensor setup was also discussed. Interrogation frequency analysis consists the minimum sampling rate to measure an AC electric field of 50/60 Hz, and also provide the electric field measurement bandwidth. the sensitivity of the proposed SIW sensor was defined and quantified as 2.3194 kHz/mV and 6.002 kHz/mV for the two varactors-loaded sensor and one varactor-loaded sensor, respectively.

Chapter 6

Conclusions

In this thesis project, the design, fabrication and assessment of a substrate-integrated-waveguide (SIW) resonator-based sensor was presented. The sensor is composed of an SIW resonator and a coupling microstrip transmission line to energize the sensor. The proposed sensor is based on a substrate-integrated waveguide (SIW) resonator. The resonator consists of an isolated circular region on the patch conductor and varactor diodes are mounted across the gap between the region and the patch. The capacitance of the varactors is a function of the reverse bias voltage applied at the terminals of the varactors. An external electric field is coupled capacitively to the isolated region and induces a voltage over the terminals of the varactors. Consequently, the induced voltage imposed a change in the capacitance of the varactor diode and accordingly the resonator. Therefore, A change in the capacitance of the resonator leads in a shift at the resonance frequency of the proposed sensor.

The sensor is designed to operate at the ISM Band of 2.4 GHz to 2.5 GHz. The measurements demonstrate that the proposed SIW resonator sensor offers a loaded quality factor of around 250. A frequency shift of up to 33 MHz is obtained for a reverse bias voltage of 0 to 5 V. The proposed sensor is passive which means there is no requirement to have batteries. Moreover, the proposed sensor is designed to operate wirelessly and can be interrogated remotely. The proposed sensor is employed to measure the AC electric field in the vicinity of the high voltage apparatus. The proposed SIW sensor is applicable in the measurement of the AC electric field, induced voltage in high/medium voltage structures and in insulation defects.

The sensor is interrogated by a fast sampling rate interrogation system. The interrogation system provides the ability to capture a time-varying AC electric field. The utilized interrogation system is capable of acquiring samples of a time-varying measurand at a rate up to 4 MHz. A radio frequency (RF) pulse close to the natural frequency of the sensor is transmitted to the sensor and once the transmitter is off, the SIW sensor starts to resonate at its natural frequency and sends back ring back signals to the interrogator. The interrogation system is composed of switches, RF sources, amplifiers, DC blocks, a low-pass filter, bi-directional coupler and a mixer to downconvert the received signals. The amplified, downconverted ring back signal is captured by an oscilloscope capable of sampling at a high rate. Next, the recorded ring back signal is used to derive the resonance frequency of the sensor perturbed by an external AC electric field. Therefore, repetitive signals captured by fast-sampling oscilloscope results in the re-construction of the applied AC induced electric field originating from the high voltage apparatus.

Two parallel plates used to generate an external electric field E_{rms}= 3 KV/m. The Variac is employed to deliver a V_{rms} =120 V to the plates where their distance is 4 cm. This measurement is used to evaluate the performance of the proposed SIW sensor.

The proposed sensor is easy to fabricate, inexpensive, and compatible with printed circuit board technology, that makes it a viable candidate for remote monitoring of high-voltage fields in hazardous situations where human contact is not desirable.

6.1 Future Work

In this thesis, the measurement results show that the proposed SIW sensor and the corresponding interrogation system is operable to derive the reconstructed AC electric field surrounding the high voltage apparatus. The reconstruction method is based on deriving the resonance frequency change caused by the AC electric field. The proposed SIW sensor and the interrogation system can be improved to enhance the measurement accuracy and decrease the limiting errors and losses occurred during the fabrication or interrogation process.

In this section, further studies to improve the proposed sensor and the interrogation system are suggested. The possible high voltage applications to evaluate the proposed sensor are presented as well:

- The proposed sensor is potentially wireless. The coaxial cable which connects the interrogation system and the proposed SIW sensor could be replaced by an antenna to investigate the far-field performance of the proposed sensor.

- Since the employed technology to fabricate the proposed sensor is printed circuit board (PCB) technology, a built-in microstrip antenna based on PCB is a viable candidate to replace the commercial antennas.

- The soldering technique is utilized to construct the metallized via posts of substrate-integrated waveguide resonator. This procedure adds inaccuracy and increases conductor loss. The proposed sensor could be fabricated using solid copper vias in order to eliminate any loss added by soldering.

- The dynamic range of the proposed sensor is pertinent to the varactor diodes and the discharge resistors. The desired dynamic range is achievable by modifying the varactors and discharge resistors.

- In order to fully understand the circuit model of the proposed sensor, further studies can be carried out to model the only non-linear component (the varactor diodes) at both low frequencies and RF frequencies.

- The bi-directional coupler of the interrogation system adds the insertion loss of -10 dB in measurements. The bi-directional coupler and the interrogation system antenna is replaceable with an antenna with circular polarization. It is possible to use x-axis to transmit RF signals to the sensor. On the other hand, the re-emitted ring back signals of the sensor could be in y-axis to be detectable by the same antenna of the interrogation system. This would add -6 dB loss in total.

- The transmitted power of the RF signal to the sensor might generate a current in the varactors resulting in a capacitance change. This shift comes from the interrogation system, not from an external measurand such as an AC electric field surrounding the high voltage apparatus. The undesired effect of the transmitted power should be investigated in order not to disturb the capacitance change of the varactor diodes.

- The proposed sensor is capable of interrogating multiple sensors simultaneously. Frequency hopping spectrum spread allows us to have more than one sensor being interrogated at the same time. This method can enhance the functionality of the interrogation system and decrease the interference of multiple frequency channels operating in the ISM band.

- Some possible applications of the proposed SIW sensor can be listed as below:

  1- Remote measurement of high/medium voltage

  2- Detection of insulation defects using its electric field profile

References

[1] Q. Tan, T. Luo, T. Wei, J. Liu, L. Lin, and J. Xiong, "A wireless passive pressure and temperature sensor via a dual lc resonant circuit in harsh environments," *Journal of Microelectromechanical Systems*, vol. 26, no. 2, pp. 351–356, April 2017.

[2] C. Liu and F. Tong, "An siw resonator sensor for liquid permittivity measurements at c band," *IEEE Microwave and Wireless Components Letters*, vol. 25, no. 11, pp. 751–753, Nov 2015.

[3] J. Yao, S. Tjuatja, and H. Huang, "Real-time vibratory strain sensing using passive wireless antenna sensor," *IEEE Sensors Journal*, vol. 15, no. 8, pp. 4338–4345, Aug 2015.

[4] V. Viikari, J. Song, and H. Seppa, "Passive wireless sensor platform utilizing a mechanical resonator," *IEEE Sensors Journal*, vol. 13, no. 4, pp. 1180–1186, April 2013.

[5] S. Bhadra, D. S. Y. Tan, D. J. Thomson, M. S. Freund, and G. E. Bridges, "A wireless passive sensor for temperature compensated remote ph monitoring," *IEEE Sensors Journal*, vol. 13, no. 6, pp. 2428–2436, June 2013.

[6] D. J. Thomson, D. Card, and G. E. Bridges, "Rf cavity passive wireless sensors with time-domain gating-based interrogation for shm of civil structures," *IEEE Sensors Journal*, vol. 9, no. 11, pp. 1430–1438, Nov 2009.

[7] P. J. Chen, S. Saati, R. Varma, M. S. Humayun, and Y. C. Tai, "Wireless intraocular pressure sensing using microfabricated minimally invasive flexible-coiled lc sensor implant," *Journal of Microelectromechanical Systems*, vol. 19, no. 4, pp. 721–734, Aug 2010.

[8] B. Zemljaric, "Calculation of the connected magnetic and electric fields around an overhead-line tower for an estimation of their influence on maintenance personnel," *IEEE Transactions on Power Delivery*, vol. 26, no. 1, pp. 467–474, Jan 2011.

[9] C. E. Lin, J.-B. Wei, C.-L. Huang, and C.-J. Huang, "A new model for transformer saturation characteristics by including hysteresis loops," *IEEE Transactions on Magnetics*, vol. 25, no. 3, pp. 2706–2712, May 1989.

[10] E. E. Barkat and D. E. Hirst, "Susceptibility of 3-phase power systems to ferro-nonlinear oscillations," *Electrical Engineers, Proceedings of the Institution of*, vol. 126, no. 12, pp. 1295–1300, December 1979.

[11] M. Yazdani, D. J. Thomson, and B. Kordi, "Passive wireless sensor for measuring ac electric field in the vicinity of high-voltage apparatus," *IEEE Transactions on Industrial Electronics*, vol. 63, no. 7, pp. 4432–4441, July 2016.

[12] M. Nowak, N. Delorme, F. Conseil, and G. Jacquemod, "A novel architecture for remote interrogation of wireless battery-free capacitive sensors," in *2006 13th IEEE International Conference on Electronics, Circuits and Systems*, Dec 2006, pp. 1236–1239.

[13] W. E. Bulst, G. Fischerauer, and L. Reindl, "State of the art in wireless sensing with surface acoustic waves," *IEEE Transactions on Industrial Electronics*, vol. 48, no. 2, pp. 265–271, Apr 2001.

[14] Y. Zhao, Y. Li, B. Pan, S.-H. Kim, Z. Liu, M. M. Tentzeris, J. Papapolymerou, and M. G. Allen, "Rf evanescent-mode cavity resonator for passive wireless sensor applications," *Sensors and Actuators A: Physical*, vol. 161, no. 1, pp. 322 – 328, 2010. [Online]. Available: http://www.sciencedirect.com/science/article/pii/S0924424710001937

[15] K. Ong, C. Grimes, C. Robbins, and R. Singh, "Design and application of a wireless, passive, resonant-circuit environmental monitoring sensor," *Sensors and Actuators A: Physical*, vol. 93, no. 1, pp. 33 – 43, 2001. [Online]. Available: http://www.sciencedirect.com/science/article/pii/S0924424701006240

[16] J. Hirokawa and M. Ando, "Single-layer feed waveguide consisting of posts for plane tem wave excitation in parallel plates," *IEEE Transactions on Antennas and Propagation*, vol. 46, no. 5, pp. 625–630, May 1998.

[17] H. Uchimura, T. Takenoshita, and M. Fujii, "Development of a ldquo;laminated waveguide rdquo;," *IEEE Transactions on Microwave Theory and Techniques*, vol. 46, no. 12, pp. 2438–2443, Dec 1998.

[18] K. Entesari, A. P. Saghati, V. Sekar, and M. Armendariz, "Tunable siw structures: Antennas, vcos, and filters," *IEEE Microwave Magazine*, vol. 16, no. 5, pp. 34–54, June 2015.

[19] F. Xu and K. Wu, "Guided-wave and leakage characteristics of substrate integrated waveguide," *IEEE Transactions on Microwave Theory and Techniques*, vol. 53, no. 1, pp. 66–73, Jan 2005.

[20] D. Deslandes and K. Wu, "Accurate modeling, wave mechanisms, and design considerations of a substrate integrated waveguide," *IEEE Transactions on Microwave Theory and Techniques*, vol. 54, no. 6, pp. 2516–2526, June 2006.

[21] M. Bozzi, A. Georgiadis, and K. Wu, "Review of substrate-integrated waveguide circuits and antennas," *IET Microwaves, Antennas Propagation*, vol. 5, no. 8, pp. 909–920, June 2011.

[22] F. Giuppi, A. Georgiadis, A. Collado, M. Bozzi, and L. Perregrini, "Tunable siw cavity backed active antenna oscillator," *Electronics Letters*, vol. 46, no. 15, pp. 1053–1055, July 2010.

[23] A. P. Saghati, M. Azarmanesh, and R. Zaker, "A novel switchable single- and multifrequency triple-slot antenna for 2.4-ghz bluetooth, 3.5-ghz wimax, and 5.8-ghz wlan," *IEEE Antennas and Wireless Propagation Letters*, vol. 9, pp. 534–537, 2010.

[24] N. Behdad and K. Sarabandi, "Dual-band reconfigurable antenna with a very wide tunability range," *IEEE Transactions on Antennas and Propagation*, vol. 54, no. 2, pp. 409–416, Feb 2006.

[25] Z. Chen, W. Hong, J. Chen, and J. Zhou, "Design of high-q tunable siw resonator and its application to low phase noise vco," *IEEE Microwave and Wireless Components Letters*, vol. 23, no. 1, pp. 43–45, Jan 2013.

[26] F. F. He, K. Wu, W. Hong, L. Han, and X. Chen, "A low phase-noise vco using an electronically tunable substrate integrated waveguide resonator," *IEEE Transactions on Microwave Theory and Techniques*, vol. 58, no. 12, pp. 3452–3458, Dec 2010.

[27] C. Zhong, J. Xu, Z. Yu, and Y. Zhu, "Ka-band substrate integratedwaveguide gunn oscillator," *IEEE Microwave and Wireless Components Letters*, vol. 18, no. 7, pp. 461–463, July 2008.

[28] Y. Cassivi and K. Wu, "Low cost microwave oscillator using substrate integrated waveguide cavity," *IEEE Microwave and Wireless Components Letters*, vol. 13, no. 2, pp. 48–50, Feb 2003.

[29] S. Nam, B. Lee, and J. Lee, "Constant-absolute-bandwidth frequency-tunable half-mode siw filter containing no tunable coupling structures," in *2017 IEEE MTT-S International Microwave Symposium (IMS)*, June 2017, pp. 267–270.

[30] M. Esmaeili and J. Bornemann, "Novel tunable bandstop resonators in siw technology and their application to a dual-bandstop filter with one tunable stopband," *IEEE Microwave and Wireless Components Letters*, vol. 27, no. 1, pp. 40–42, Jan 2017.

[31] H. J. Tang, W. Hong, Z. C. Hao, J. X. Chen, and K. Wu, "Optimal design of compact millimetre-wave siw circular cavity filters," *Electronics Letters*, vol. 41, no. 19, pp. 1068–1069, September 2005.

[32] D. D. Zhang, L. Zhou, L. S. Wu, L. F. Qiu, W. Y. Yin, and J. F. Mao, "Novel bandpass filters by using cavity-loaded dielectric resonators in a substrate integrated waveguide," *IEEE Transactions on Microwave Theory and Techniques*, vol. 62, no. 5, pp. 1173–1182, May 2014.

[33] V. Sekar, M. Armendariz, and K. Entesari, "A 1.2 x2013;1.6-ghz substrate-integrated-waveguide rf mems tunable filter," *IEEE Transactions on Microwave Theory and Techniques*, vol. 59, no. 4, pp. 866–876, April 2011.

[34] S. Adhikari, A. Ghiotto, S. Hemour, and K. Wu, "Tunable non-reciprocal ferrite loaded siw phase shifter," in *2013 IEEE MTT-S International Microwave Symposium Digest (MTT)*, June 2013, pp. 1–3.

[35] A. Nafe and A. Shamim, "An integrable siw phase shifter in a partially magnetized ferrite ltcc package," *IEEE Transactions on Microwave Theory and Techniques*, vol. 63, no. 7, pp. 2264–2274, July 2015.

[36] P. Yadav, S. Mukherjee, and A. Biswas, "Design of planar substrate integrated waveguide (siw) phase shifter using air holes," in *2015 IEEE Applied Electromagnetics Conference (AEMC)*, Dec 2015, pp. 1–2.

[37] Y. J. Cheng, Q. D. Huang, Y. R. Wang, and J. L. W. Li, "Narrowband substrate integrated waveguide isolators," *IEEE Microwave and Wireless Components Letters*, vol. 24, no. 10, pp. 698–700, Oct 2014.

[38] F. Fesharaki, C. Akyel, and K. Wu, "Broadband substrate integrated waveguide edge-guided mode isolator," *Electronics Letters*, vol. 49, no. 4, pp. 269–271, Feb 2013.

[39] Q. Li, X. Guo, H. Song, K. K. Li, Y. K. Zou, H. Jiang, and A. Gopinath, "60ghz substrate integrated waveguide resonance isolator," in *2016 IEEE MTT-S International Microwave Symposium (IMS)*, May 2016, pp. 1–3.

[40] S. Hemour, S. Adhikari, A. Ghiotto, and K. Wu, "Low magnetic biased siw-based isolator: Effect of the rising temperature on the performance of the isolator," in *WAMICON 2014*, June 2014, pp. 1–3.

[41] M. Armendariz, V. Sekar, and K. Entesari, "Tunable siw bandpass filters with pin diodes," in *The 40th European Microwave Conference*, Sept 2010, pp. 830–833.

[42] S. Sirci, J. D. Martnez, M. Taroncher, and V. E. Boria, "Varactor-loaded continuously tunable siw resonator for reconfigurable filter design," in *2011 41st European Microwave Conference*, Oct 2011, pp. 436–439.

[43] S. Adhikari, A. Ghiotto, and K. Wu, "Simultaneous electric and magnetic two-dimensional tuning of substrate integrated waveguide cavity resonator," in *2012 IEEE/MTT-S International Microwave Symposium Digest*, June 2012, pp. 1–3.

[44] F. Mira, J. Mateu, and C. Collado, "Mechanical tuning of substrate integrated waveguide resonators," *IEEE Microwave and Wireless Components Letters*, vol. 22, no. 9, pp. 447–449, Sept 2012.

[45] A. Anand, J. Small, D. Peroulis, and X. Liu, "Theory and design of octave tunable filters with lumped tuning elements," *IEEE Transactions on Microwave Theory and Techniques*, vol. 61, no. 12, pp. 4353–4364, Dec 2013.

[46] A. Sarkar, A. Sharma, M. Adhikary, A. Biswas, and M. J. Akhtar, "Bi-directional siw leaky-wave antenna using te20 mode for frequency beam scanning," *Electronics Letters*, vol. 53, no. 15, pp. 1017–1019, 2017.

[47] R. B. Northrop, *Introduction to Instrumentation and Measurements*, second edition ed. Taylor & Francis Group, 2005.

[48] B. Bahreyni, G. Wijeweera, C. Shafai, and A. Rajapakse, "Analysis and design of a micromachined electric-field sensor," *Journal of Microelectromechanical Systems*, vol. 17, no. 1, pp. 31–36, Feb 2008.

[49] R. N. DeanJr. and A. Luque, "Applications of microelectromechanical systems in industrial processes and services," *IEEE Transactions on Industrial Electronics*, vol. 56, no. 4, pp. 913–925, April 2009.

[50] G. Wijeweera, B. Bahreyni, C. Shafai, A. Rajapakse, and D. Swatek, "Micromachined electric field sensor to measure ac and dc fields in power systems," in *2009 IEEE Power Energy Society General Meeting*, July 2009, pp. 1–1.

[51] P. S. Riehl, K. L. Scott, R. S. Muller, R. T. Howe, and J. A. Yasaitis, "Electrostatic charge and field sensors based on micromechanical resonators," *Journal of Microelectromechanical Systems*, vol. 12, no. 5, pp. 577–589, Oct 2003.

[52] P. Yang, C. Peng, H. Zhang, S. Liu, D. Fang, and S. Xia, "A high sensitivity soi electric-field sensor with novel comb-shaped microelectrodes," in *2011 16th International Solid-State Sensors, Actuators and Microsystems Conference*, June 2011, pp. 1034–1037.

[53] R. Moghe, A. R. Iyer, F. C. Lambert, and D. M. Divan, "A low-cost wireless voltage sensor for monitoring mv/hv utility assets," *IEEE Transactions on Smart Grid*, vol. 5, no. 4, pp. 2002–2009, July 2014.

[54] R. Moghe, A. Iyer, F. C. Lambert, and D. Divan, "A robust smart sensor for smart substations," in *2012 IEEE Power and Energy Society General Meeting*, July 2012, pp. 1–8.

[55] W. McNulty, "Voltage detection and indication by electric field measurement," in *2011 IEEE PES 12th International Conference on Transmission and Distribution Construction, Operation and Live-Line Maintenance (ESMO)*, May 2011, pp. 1–6.

[56] M. A. Noras and A. Pandey, "Surface charge density measurements," *IEEE Industry Applications Magazine*, vol. 16, no. 4, pp. 41–47, July 2010.

[57] M. A. Noras, "Electric field sensor based on a varactor diode/mis/mos structure," in *2010 IEEE Industry Applications Society Annual Meeting*, Oct 2010, pp. 1–3.

[58] F. Yu, K. G. Lyon, and E. C. Kan, "A novel passive rfid transponder using harmonic generation of nonlinear transmission lines," *IEEE Transactions on Microwave Theory and Techniques*, vol. 58, no. 12, pp. 4121–4127, Dec 2010.

[59] B. G. Colpitts and G. Boiteau, "Harmonic radar transceiver design: miniature tags for insect tracking," *IEEE Transactions on Antennas and Propagation*, vol. 52, no. 11, pp. 2825–2832, Nov 2004.

[60] V. Viikari, H. Seppa, and D. W. Kim, “Intermodulation read-out principle for passive wireless sensors,” *IEEE Transactions on Microwave Theory and Techniques*, vol. 59, no. 4, pp. 1025–1031, April 2011.

[61] S. Bhadra, W. Blunt, C. Dynowski, M. McDonald, D. J. Thomson, M. S. Freund, N. Cicek, and G. E. Bridges, “Fluid embeddable coupled coil sensor for wireless ph monitoring in a bioreactor,” *IEEE Transactions on Instrumentation and Measurement*, vol. 63, no. 5, pp. 1337–1346, May 2014.

[62] Y. Yan, Z. Zeng, C. Chen, H. Jiang, Z. y. Chang, D. M. Karabacak, and M. A. P. Pertijs, “An energy-efficient reconfigurable readout circuit for resonant sensors based on ring-down measurement,” in *IEEE SENSORS 2014 Proceedings*, Nov 2014, pp. 221–224.

[63] D. J. Thomson, D. Card, and G. E. Bridges, “Rf cavity passive wireless sensors with time-domain gating-based interrogation for shm of civil structures,” *IEEE Sensors Journal*, vol. 9, no. 11, pp. 1430–1438, Nov 2009.